Characterization of a novel β-cyclodextrin polymer for the removal of organic micropollutants from aqueous solution

A Thesis

Presented to the Faculty of the Graduate School

of Cornell University

in Partial Fulfillment of the Requirement for the Degree of

Master of Science

by

Yuhan Ling

August 2016

Table of Contents

ABSTRACT

Organic micropollutants (MPs) are difficult to remove from water and wastewater in a cost-effective and energy efficient manner. In this research, a novel β-cyclodextrin polymer (P-CDP) was investigated as a potential adsorbent of MPs and its performance was benchmarked against a common coconut-shell based granular activated carbon (CCAC). Adsorption kinetics were measured in batch and filtration-type experiments and distribution coefficients were determined from affinity experiments that investigated 90 structurally diverse MPs in a complex mixture and at environmentally relevant concentrations. The batch kinetic data was used to estimate pseudo second-order rate constants (k_{obs}) for 83 of the 90 MPs based on a conventional kinetic model. The k_{obs} for 70 of the 83 MPs were orders-of-magnitude greater for P-CDP than CCAC, indicating that adsorption equilibrium of P-CDP can be achieved relatively rapidly. However, overall batch removal was greater for most MPs on the CCAC, indicating a relatively greater adsorption capacity for CCAC. The filtration experiments showed that instant uptake on the P-CDP was greater than 90% for 31 of the MPs, confirming the potential for rapid MP uptake. However, the remaining MPs were only partially removed revealing an apparent selectivity of the P-CDP. Therefore, the distribution coefficient (K_∞) was determined for each MP in an affinity experiment and the data were used to develop a Linear Solvation Energy Relationship (LSER). The coefficients of the resulting LSER model suggest that the McGowan volume of a particular MP is an important factor influencing adsorption affinity for P-CDP but positive charges can also influence the adsorption of MPs when the McGowan volume ranges from 0.87 to 5.73 ($cm^3\ mol^{-1}/100$). Together, data from these experiments provide key insights into the mechanisms by which MPs bind to P-CDP and demonstrate that the P-CDP could be a suitable alternative to activated carbon with potential applications in water and wastewater treatment.

BIOGRAPHICAL SKETCH

Yuhan Ling was born in Nantong, China in 1991. He graduated with a degree in Environmental Science and Engineering and a degree in International Trade and Economics from Shanghai Jiang Tong University in 2014. As an undergraduate student, he was the director of the Youth Voluntary Department and worked to popularize the concepts of environmental protection and sustainable development. His experiences in environmental engineering include a half-year internship as an assistant engineer in the EHS department of Cargill Investments (China) Ltd., a two-month internship as an environmental consultant in Leopard Imaging (CA) Ltd., a one-year lab research on Fenton-like catalysts in the Long research group at Shanghai Jiao Tong University and Rice University, and a one-year lab research on Ultramembranes in the Shao research group at Shanghai Jiao Tong University. In August 2014, he entered Cornell University and started his study towards the M.S. Degree in Environmental Engineering. In February 2016, he received and accepted the offer to continue as a Ph.D. candidate in the Helbling research group.

ACKNOWLEDGEMENT

In the first place, I would like to give my sincere thanks to the School of Civil and Environmental Engineering at Cornell University. It is my great honor to continue as a graduate student in such an outstanding School. And this is where I am blessed with the precious opportunity to meet my advisor Dr. Helbling. When I joined the Helbling research group, I was trusted with the chance to work on a great collaborative project regarding a novel cyclodextrin polymer. During the research, he presents the operation of HPLC-MS to me step-by-step with great patience; every time I came up with experimental difficulties, he can offer me the most appropriate and thoughtful methods to solve the problems. Benefiting from the guidance and selfless dedication of Dr. Helbling, not only can I master the operations of many advanced lab instruments and data processing and graphing software, I also learned how to come up with the considerable plans to solve practical problems in research and got a clear vision of my future. In the near future, I will continue as a Ph.D. candidate in the Helbling research group and I believe that I will be able to grow into a qualified environmental engineer under the instructions of Dr. Helbling.

At the same time, I would like to give my sincere thanks to our collaborators, Dr. Dichtel and the postdocs and graduate students in the Dichtel research group: Dr. Alsbaiee, Dr. Smith, Leilei Xiao and Max Klemes. Due to the invention of this novel polymer by these chemists, I can conduct my M.S. research to study the efficacy of this polymer in water treatment which is the topic in which I am most interested. Hereby, I would like to give my special thanks to Dr. Dichtel for his luminous suggestions for this research, to Dr. Alsbaiee and Dr. Smith for their preparation of this novel cyclodextrin polymer, to Leilei Xiao for her work on the

characterization of the surface area, pore size distribution, elemental analysis and FT-IR for the polymer and coconut-shell based activated carbon.

In the second place, I would like to give my sincere thanks to Dr. Bisogni for serving as my minor advisor. His experienced suggestions helped me a lot during the research.

致谢

首先，我要感谢康奈尔大学土木与环境工程学院，正因为有幸在这样一个治学严谨，师资背景雄厚的学院继续我的研究生学习， 我才能在提升了自己的学术水准的同时有幸遇到我的导师，赫柏林博士（Dr. Helbling）。我在这所古老而享有盛誉的大学最幸运的事情便是能加入赫柏林实验组。相识之初，我的导师便给予了我充分的信任，让我加入了一个关于新型吸附材料的重要合作项目； 在研究中，他亲历亲为， 为我演示如何使用高性能四极杆-轨道阱高效液相色谱-质谱联用系统；在实验过程中，我遇到过很多技术方面的棘手问题，他都在第一时间用最周全的方法为我解决困难。得益于赫柏林博士的悉心指导和无私奉献，我不仅熟练掌握了各种先进实验仪器和数据处理及绘图系统的操作方法，学会了如何自主思考和解决实际的科研问题，更明了了自己的人生规划。在未来的日子里，我将留在赫柏林实验组继续我的博士学习。我相信在赫柏林博士的指导下，我一定可以再接再厉，成长为一个合格而优秀的环境学者。

与此同时，我要感谢我们的项目合作方，迪希特尔博士（Dr. Dichtel）和其实验组的研究生们：阿拉丁博士（Dr. Alsbaiee)，布莱恩博士（Dr. Smith），肖蕾蕾和马克思。才华横溢的他们在迪希特尔博士的带领下，发明了一种新型的环糊精聚合物，正因为此，我才有机会在我热爱的水处理领域进行相关的吸附研究。在此，特别感谢迪希特尔博士在研究过程中提供的建议和帮助；感谢阿拉丁博士和布莱恩博士为相关实验制备的环糊精聚合物样品；感谢肖蕾蕾提供的有关比表面积，孔径分布以及傅里叶红外的表征数据，相关图谱以及分析性文字。

其次，我要感谢我的另一位导师，比索尼博士（Dr. Bisogni）。他所提供的有关吸附实验的相关建议令我获益匪浅。于此，我对他表示最诚挚的谢意。

最后，我要感谢我的家人，朋友和实验室的每一位成员。他们在生活和学习中给我的鼎力支持是我坚持不懈的动力。在未来的日子里，希望我们能并肩携手，为我们身边的环保事业贡献出自己的力量！

LIST OF TABLES

LIST OF FIGURES

CHAPTER 1: INTRODUCTION

1.1 Context

There are more than 84,000 synthetic organic chemicals registered for industrial and consumer use in the United States under the Toxic Substances Control Act (TSCA). Decades of environmental monitoring have proven that the ultimate fate of many of these chemicals is to the aquatic environment.[1–3] Of particular concern are the groups of persistent and bioactive compounds such as pharmaceuticals, pesticides, personal care products, and flame retardants.[4–7] These types of chemicals are transported to water resources through diffuse runoff from agricultural and urban landscapes or through point-source discharges of wastewater and stormwater. Though the concentration of these so-called micropollutants (MPs) in water resources are at low levels (ng/L to µg/L), emerging data has shown a variety of ecosystem effects.[3,8,9] There is also emerging concern over human exposure to MPs in municipal drinking water.[10]

Conventional water and wastewater treatment processes only partially remove most polar and semi-polar MPs. Conventional particle removal processes including coagulation, flocculation, and sedimentation only remove very nonpolar MPs and most pesticides and pharmaceuticals remain partitioned in the aqueous phase.[11–15] Granular media filtration can contribute to some MP removal when the media is allowed to become bioactive, though removal is incomplete at best.[16–19] Chemical oxidation and disinfection can transform many MPs, though there is emerging concern over the formation of new disinfection byproducts.[2,12,20–22] With respect to wastewater treatment, activated sludge treatment can at least partially remove some MPs, though complete removal is rare and many MPs are completely recalcitrant during conventional wastewater treatment.[21,23,24]

Because conventional water and wastewater treatment processes do not remove MPs efficiently, a variety of advanced treatment processes have been investigated for their potential to remove MPs from water. For example, ozonation and some advanced oxidation processes (AOPs) including Fenton catalysis, UV/H_2O_2, and UV/TiO_2 have been demonstrated to be effective in the degradation of many MPs.[24–28] However, there are well-known disadvantages of ozonation and AOPs that lead to some concerns.[29] For example, oxidation processes frequently result in the formation of MP transformation products (TPs) which can retain biological activity and at times be even more toxic than the parent MP.[30–32] In addition, oxidation TPs can be more resistant to downstream biodegradation and ultimately be more persistent than the parent MP.[20] Besides the formation of oxidation TPs, ozonation and AOPs are relatively expensive processes because photo radiation and the generation of ozone are energy intensive and they consume chemical reagents including catalysts and oxidizers.[24,33] Another emerging alternative is membrane filtration including nanofiltration (NF) and reverse osmosis (RO), which has recently been demonstrated to be an effective barrier for most MPs due to the high efficiency afforded by the mechanism of size exclusion.[34,35] However, removal by NF and RO favors uncharged MPs, a small constituent of MPs, and does not remove charged MPs efficiently. Further, the operation of NF and RO are also energy intensive and requires significant maintenance costs due to fouling and upkeep of the NF and RO membrane.[36–38] Clearly, more cost effective and efficient means for MP removal from water are needed.

Adsorption processes are often considered to be a more cost-effective and less energy-intensive means for the removal of MPs from water, though conventional activated carbon (AC) adsorption is not without its own drawbacks. AC is currently the most widespread adsorbent used to remove organic chemicals during water and wastewater treatment.[6,16,17,19,39–41] AC is

inexpensive and widely available throughout the world. Its efficacy derives from its high surface area, hydrophobic surfaces, and high microporosity that enable binding with organic molecules primarily through hydrophobic interactions. However, there are several aspects of AC that limit its utility in removing trace MPs from water. First, the adsorption kinetics on AC are relatively slow due to the diffusion controlled transport in the AC pores. This property results in the long time (on the orders of days to weeks) for AC to reach adsorption equilibrium with trace MPs.[6,19] Second, adsorption by AC is nonselective, and as such background natural organic matter (NOM) generally present in natural waters can also be adsorbed which will reduce the adsorption capacity of the AC for MPs.[18] Third, many relatively hydrophilic MPs and positively charged MPs (at neutral pH) cannot be effectively removed by GAC. Finally, the regeneration of spent activated carbon requires incineration at high temperatures and does not fully restore adsorption performance.[42] New adsorbents that address these deficiencies of ACs could lead to more efficient removal of MPs from water and wastewater.

The research in this thesis explores a novel porous β-cyclodextrin (β-CD) containing polymer (P-CDP) recently discovered at Cornell University.[7] The structural information of β-CD and P-CDP can be found in Table 1. The P-CDP was previously demonstrated to outperform Norit activated carbon (one of the best commercially available activated carbon materials) for the removal of several model MPs and other organic molecules. Results from these initial studies of the new P-CDP are promising, however much more data are needed to understand the potential of this material for the removal of complex mixtures of MPs during water or wastewater treatment. The objectives of this research were to: (i) characterize the performance of P-CDP for the removal of 90 MPs from water at environmentally relevant concentrations; and (ii) benchmark its performance against a conventional AC adsorbent.

Table 1. Schematic of β-CD monomer, P-CDP network, and photograph showing particle morphology.

A. β-CD Monomer	B. P-CDP: Networks	C. P-CDP: Morphology
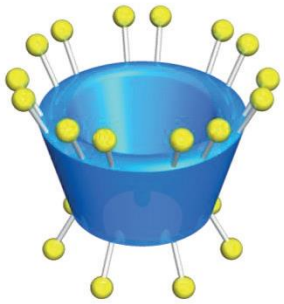	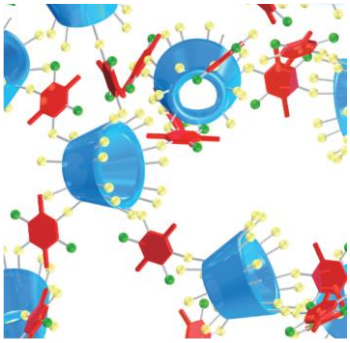	

1.2 Research questions

The experiments, data analysis, and modelling work described in this thesis were aimed at improving the fundamental understanding of MP adsorption on the P-CDP at environmentally relevant concentrations. A series of experiments were designed to investigate the adsorption kinetics and affinity of 90 MPs to both P-CDP and a commercially available AC to address the following research questions:

1. What is the relative uptake of each MP on P-CDP or CCAC in batch adsorption contactors?
2. What is the relative uptake of each MP on P-CDP or CCAC in filtration-type reactors?
3. What physicochemical properties determine the uptake affinity of MPs on P-CDP?

CHAPTER 2: THE BATCH KINETICS, INSTANTANEOUS UPTAKE, AND SELECTIVITY OF A NOVEL β-CYCLODEXTRIN POLYMER FOR THE REMOVAL OF MICROPOLLUTANTS FROM AQUEOUS SOLUTION

2.1 Abstract

Organic micropollutants (MPs) are difficult to remove from water and wastewater in a cost-effective and energy efficient manner. In this research, a novel β-cyclodextrin polymer (P-CDP) was investigated as a potential adsorbent of MPs and its performance was benchmarked against a common coconut-shell based granular activated carbon (CCAC). Adsorption kinetics were measured in batch and filtration-type experiments and distribution coefficients were determined from affinity experiments that investigated 90 structurally diverse MPs in a complex mixture and at environmentally relevant concentrations. The batch kinetic data was used to estimate pseudo second-order rate constants (k_{obs}) for 83 of the 90 MPs based on a conventional kinetic model. The k_{obs} for 70 of the 83 MPs were orders-of-magnitude greater for P-CDP than CCAC, indicating that adsorption equilibrium of P-CDP can be achieved relatively rapidly. However, overall batch removal was greater for most MPs on the CCAC, indicating a relatively greater adsorption capacity for CCAC. The filtration experiments showed that instant uptake on the P-CDP was greater than 90% for 31 of the MPs, confirming the potential for rapid MP uptake. However, the remaining MPs were only partially removed revealing an apparent selectivity of the P-CDP. Therefore, the distribution coefficient (K_∞) was determined for each MP in an affinity experiment and the data were used to develop a Linear Solvation Energy Relationship (LSER). The coefficients of the resulting LSER model suggest that the McGowan volume of a

particular MP is an important factor influencing adsorption affinity for P-CDP but positive charges can also influence the adsorption of MPs when the McGowan volume ranges from 0.87 to 5.73 (cm^3 mol^{-1}/100). Together, data from these experiments provide key insights into the mechanisms by which MPs bind to the P-CDP and demonstrate that the P-CDP could be a suitable alternative to activated carbon with potential applications in water and wastewater treatment.

2.2 Introduction

The poor removal of some trace organic chemicals (*i.e.*, micropollutants, MPs) during conventional drinking water and wastewater treatment has raised concerns about potential adverse effects on aquatic ecosystems and human health.[3,8–10,14,15,21,23,24] Of particular concern are the groups of persistent and bioactive compounds such as pharmaceuticals, pesticides, personal care products, and flame retardants[4–7] which can have effects on sensitive aquatic organisms even at low levels (ng/L to µg/L). For example, it has been observed that endocrine-disrupting compounds (EDCs) including atrazine, estrone, and testosterone can cause intersex, reproductive complications, and feminization of males among fish and mussel populations.[43,44] Additionally, human exposure to MPs is expected to occur through drinking water derived from sources that are impacted by wastewater discharges due to the persistence of MPs in conventional drinking water treatment. Also, MPs such as EDCs even at trace levels can pose potential risks to public health.[45] Therefore, the release of MPs into surface waters should be reduced.

To upgrade conventional wastewater treatment plants for the removal of MPs, numerous studies investigating advanced techniques have been conducted. Currently, some tertiary treatment processes have been demonstrated to be effective for the removal of MPs including ozonation and advanced oxidation processes (AOPs),[24–28] nanofiltration (NF) and reverse osmosis (RO),[34,35] and activated carbon adsorption.[6,19,21,46] Among these techniques, adsorption onto activated carbon (AC) has been identified as one of the best options in terms of MP removal without the formation of byproducts along with treatment efficiency and cost.[21]

AC is the most widespread adsorbent used to remove organic chemicals during water and wastewater treatment and also presents the potential to remove MPs.[6,16,17,19,39–41] The efficacy of

AC derives from its high surface area, hydrophobic surfaces, and high microporosity that enables binding with organic molecules primarily through hydrophobic interactions. In previous studies, it has been demonstrated that a broad spectrum of MPs can be removed efficiently with powdered activated carbon (PAC) in batch adsorption contactor processes followed by ultrafiltration (UF).[21] PAC-UF treatment was also suggested as the most suitable option for sensitive receiving waters due to the great reduction of effluent toxicity.[21,47] As another important application of AC, granular activated carbon (GAC) packed column filtration has been demonstrated to have potential for the control of MPs and has been applied in some water and wastewater treatment plants.[19] However, there are several aspects of AC that limit its utility in removing trace MPs from water. First, the adsorption kinetics of AC are relatively slow due to the diffusion controlled transport in the AC pores. This property results in the long time (on the orders of days to weeks) for AC to reach adsorption equilibrium with trace MPs.[6,19] Second, adsorption by AC is nonselective, and, as such, background natural organic matter (NOM) generally present in water can also be adsorbed which will reduce the adsorption capacity of the AC and the kinetics of MP uptake through direct-site-competition and pore-blockage mechanisms.[18] Third, many relatively hydrophilic MPs and positively charged MPs (at neutral pH) cannot be effectively removed by GAC.[48–50] Finally, the regeneration of spent activated carbon requires incineration at high temperatures and does not fully restore performance.[42]

As a consequence of these deficiencies of ACs, some recent studies have explored the optimization of conventional AC treatment processes or alternative adsorbents for MP removal. For example, Bonvin et al.[46] demonstrated that the faster kinetics of super-fine PAC (SPAC), as compared with regular-sized PAC, can reduce the necessary contact time and contact tank size as well as the dosing requirements for specific targeted MP removal in PAC-UF treatment.

However, fouling problems caused by natural organic matter (NOM) were found to be worse for SPAC than PAC. Rossner et al.[6] compared the effectiveness of three alternative adsorbents, including a carbonaceous resin and two high-silica zeolites, with a coconut-shell based GAC (CCAC). Low cost adsorbents such as fruit wastes, sawdust and other wood type materials, rice husks, petroleum wastes, fertilizer wastes, chitosan and seafood processing wastes, clays, sediment and soil, and ore minerals were also investigated to assess their capabilities in the removal of MPs.[51] Though these alternative adsorbents showed removal for some MPs, none of them can compete with AC when it comes to the removal efficiency and effectiveness.

β-cyclodextrin (β-CD), is an inexpensive, sustainably produced macrocycle of glucose and was demonstrated in previous studies to encapsulate organic molecules within its cavity to form stable host-guest complexes.[52] As a result, β-CD has been investigated for the design of pharmaceutical carriers, chemical stabilizers, and adsorbents.[22,53,54] Though the β-CD monomer is soluble in water, it can be crosslinked with organic compounds (e.g., epichlorohydrin) to generate insoluble polymers without the loss of complex-formation capability. For example, the epichlorohydrin crosslinked polymer (EPI-CDP) is a commercially available adsorbent used to sequester organic molecules in aqueous solutions with high affinity. Despite the strong affinity and binding strength of the EPI-CDP, it generally performs poorly as an adsorbent (slow kinetics and low capacity) relative to activated carbon due to its low surface area (<30 m^2 g^{-1}).[7]

A novel porous β-CD containing polymer (P-CDP), with significantly improved surface area (>200 m^2 g^{-1}) and high porosity, was recently derived from a nucleophilic aromatic substitution of the hydroxyl groups of β-CD by tetrafluoroterephthalonitrile.[7] The P-CDP combines the binding affinity of β-CD[52,54,55] with the high-surface area of activated carbon to produce a broad-spectrum adsorbent for organic contaminants with superior adsorption kinetics and high capacity.

The P-CDP was demonstrated to perform better than Norit AC, which is one of the best commercially available activated carbon materials[21,46,47,56], with faster uptake kinetics and better instantaneous removal for several model organic molecules. Results from these initial studies of the new P-CDP are promising, however much more data is needed to understand the potential of this material for the removal of MPs during water or wastewater treatment. The objectives of this research were to: (i) characterize the performance of P-CDP for the removal of 90 MPs from water at environmentally relevant concentrations; and (ii) benchmark its performance against a conventional AC adsorbent. To target the objectives and research questions of interest, a set of experiments were performed to: (1) benchmark the uptake of each MP on P-CDP against CCAC in batch adsorption contactors at environmentally relevant concentrations; (2) benchmark the uptake of each MP on P-CDP against CCAC in filtration-type reactors at environmentally relevant concentrations; and (3) determine the physicochemical properties which impact the uptake affinity of MPs on P-CDP.

2.3 Materials and Methods

2.3.1 Materials

All experiments were performed with nanopure water produced by a Milli-Q system and at neutral pH. A total of 90 MPs were selected based on their environmental relevance,[1,4,5,57,58] their previous investigation for adsorption onto activated carbon,[6,18,19,22,39] and their broad range of physicochemical properties including polarity, charge state, and molecular volume. Detailed information on each MP can be found in Table A1 located in Appendix A. Stock solutions of each chemical were prepared at a concentration of 1 g/L using 100% HPLC-grade methanol with the exception of penciclovir which was prepared in Milli-Q water. The stock solutions were used to prepare analytical mixes at a concentration of 10 mg/L using Milli-Q water. The analytical mix contained all 90 MPs and was used for the kinetics experiments, the instantaneous uptake experiments and the affinity experiments. The stock solutions and the analytical mixes were stored in a freezer at -20°C and a refrigerator at 4°C, respectively.

Two adsorbents were investigated in this research: a porous β-CD-containing polymer (P-CDP) synthesized according to a published nucleophilic aromatic substitution method;[7] and a coconut-shell based GAC (CCAC, AquaCarb 1230C, Westates Carbon, Siemens, Roseville, MN). Information about surface area, pore size distribution, and FT-IR spectra for P-CDP and CCAC can be found in Appendix B. To increase the similarity in particle size between the P-CDP and the CCAC and to enhance the adsorption rate of CCAC in batch experiments, the CCAC was pulverized with a mortar and pestle until >95% (mass) passed a 74-μm sieve (200 U.S. mesh). The CCAC that remained on the sieve was remixed with the CCAC that passed through the sieve to get an unbiased mixture and to prevent any physicochemical differences

between the two fractions.[6] The P-CDP and the pulverized CCAC were dried under vacuum in a desiccator for one week and stored in a refrigerator at 4°C.

2.3.2 Batch kinetics experiments

The batch kinetics experiments were performed in 125 ml glass Erlenmeyer flasks with magnetic stir bars. For both P-CDP and CCAC, the experiments were conducted at 23°C on a multi-position stirrer (VWR) with the stirring rate at 400 revolutions per minute (rpm). The adsorbent dose was 10 mg/L and the MPs were spiked to generate an initial concentration of each adsorbate of 1 μg/L. The doses were chosen according to previous research on the same CCAC.[6]

To restore the full capacity of the vacuum-dried adsorbents, 10 mg of adsorbent (P-CDP or CCAC) was added into a 20 ml amber vial with 10 ml Milli-Q water to yield a 1 g/L suspension and then mixed with a vortex mixer (Fisher Scientific) for 30 seconds. The suspension was sonicated for 1 minute to break small aggregates and then stirred on a multi-position stirrer for 30 minutes at 360 rpm. Following this restoration procedure, 98 ml of Milli-Q water, 1 ml of the analytical mix (100 μg/L), and 1 ml of the adsorbent suspension were added to a flask successively. The adsorbent suspension was added after the addition of MPs to simulate the real situation in water or wastewater treatment. Samples were collected in 8 mL volumes at predetermined sampling times (0, 0.05, 0.17, 0.5, 1, 5, 10, 30, 60, 90, 120 minutes) and filtered with a 0.22 μm PVDF syringe filter (Restek). Control experiments to account for other MP losses were performed in the same condition with no addition of adsorbent and samples were collected at 120 minutes. All batch kinetics experiments (including controls) were performed with 5 replicates.

All samples were analyzed as described below to determine the aqueous phase concentration of each MP as a function of time.

The concentration of MPs on the solid phase was the determined by the following equation:

$$q_t = \frac{C_0 - C_t}{C_A} \quad (1)$$

where q_t (mg g^{-1}) is the amount of a MP adsorbed on the solid phase at any time t; C_0 (ng l^{-1}) is the average concentration of a MP in the samples of the control experiments; C_t (ng l^{-1}) is the concentration of a MP in the liquid phase at any sample time t; and C_A (mg l^{-1}) is the concentration of adsorbent. The batch kinetics of each adsorbent can then be described with Ho and McKay's pseudo-second-order adsorption model[59] in a linearized form as the following equation:

$$\frac{t}{q_t} = \frac{t}{q_e} + \frac{1}{k_{obs} q_e^2} \quad (2)$$

where q_e (mg g^{-1}) is the amount of a MP adsorbed on the solid phase at equilibrium; and k_{obs} (g mg^{-1} min^{-1}) is the rate constant of adsorption. Values for k_{obs} were estimated at t=30 minutes for all MPs and for both adsorbents.

The MP removal efficiency was determined by the following equation:

$$MP\ Removal = \frac{C_0 - C_t}{C_0} \times 100 \quad (3)$$

MP Removal was calculated for each of the five replicate experiments at t = 5 minutes and t = 30 minutes and is reported as the average value plus/minus the standard deviation.

2.3.3 Instantaneous uptake experiments

Instantaneous uptake experiments were performed with a 10 ml Luer-Lock tip glass syringe and Whatman 0.2 μm inorganic syringe filters at 23°C with a constant flow rate of 25 ml/min as previously described.[7] Briefly, the vacuum-dried adsorbents were prepared in the same way as was described for the batch kinetics experiments to generate a restored adsorbent suspension at a concentration of 1 g/L. The syringe filters were loaded with adsorbent by passing 0.3 mL of the activated suspension through the inorganic syringe filter to form a thin layer of 0.3 mg of adsorbent on the filter surface. Following loading of the filters with adsorbent, 8 mL of the analytical mix (1 μg/L) was pushed through the adsorbent-loaded filter with constant pressure over 20 s. Control experiments were performed in the same way with no adsorbent on the filter to account for losses through the filter itself. All instantaneous uptake experiments (including controls) were conducted in triplicate.

The filtrates were analyzed as described below to determine the aqueous phase concentration of each MP. The instant removal of MPs (in %) was then determined by the following equation:

$$MPs\ Removal = \frac{C_0 - C_I}{C_0} \times 100 \quad (4)$$

where C_0 (ng l^{-1}) is the average concentration of a MP in the samples of control experiments; and C_I (ng l^{-1}) is the concentration of a MP in the filtrate. MP Removal was calculated for each of the three replicate experiments and is reported as the average value plus/minus the standard deviation.

2.3.4 Affinity experiments

Affinity experiments were carried out using a P-CDP dose of 100 mg/L and initial concentrations of each adsorbate of 1 μg/L. The adsorbent and adsorbate doses were selected based on the results of the batch kinetics experiments and are expected to yield suitable estimates of the distribution coefficient (K_∞) for each MP. Experiments were performed in 125 ml glass Erlenmeyer flasks with magnetic stir bars at 23°C on a multi-position stirrer (VWR) with the stirring rate at 400 rpm.

In the affinity experiments, the vacuum-dried adsorbents were prepared in the same way as was described for the batch kinetics experiments to generate a 10 g/L adsorbent suspension. Aliquots of the activated adsorbent suspension were added to flasks containing a fixed volume of the analytical mix (100 μg/L) and Milli-Q water to generate experimental solutions with initial MP concentrations of 1 μg/L per compound and a P-CDP dose of 100 mg/L. Experiments were mixed for 45 minutes to allow the suspension to reach equilibrium with the MPs. Samples were collected in 8 mL volumes at 45 minutes and filtered with a 0.22 μm PVDF syringe filter (Restek). Control experiments were performed under the same conditions with no addition of adsorbent and samples were collected at 45 minutes. Affinity experiments were performed in 5 replicates.

The samples were analyzed as described below to determine the equilibrium aqueous phase concentration of each MP. The equilibrium concentration of MPs on the solid phase was determined by the following equation:

$$q_e = \frac{C_0 - C_e}{C_A} \tag{5}$$

where q_e (mg g^{-1}) is the amount of a MP adsorbed on the solid phase at equilibrium; C_0 (ng l^{-1}) is the average concentration of a MP in the samples of the control experiments; C_e (ng l^{-1}) is the average concentration of a MP in the liquid phase at equilibrium; and C_A (mg l^{-1}) is the concentration of adsorbent. The distribution coefficient K_∞ can then be determined as:

$$K_\infty = \frac{q_e}{C_e} \tag{6}$$

2.3.5 Linear Solvation Energy Relationships

2.3.5.1 Form of Linear Solvation Energy Relationship model

A Linear Solvation Energy Relationship (LSER) model has been applied to the resulting dataset that described the affinity of a set of MPs to the β-CD polymer in an aqueous solution. The form of the LSER[60] is:

$$\log K_\infty = a\alpha^H + b\beta^H + p\pi^H + rR + vV + c \tag{7}$$

where K_∞ is the distribution coefficient and model response parameter that represents the affinity of an organic solute to the adsorbent (P-CDP) at infinite dilution which can be calculated for each MP based on the equilibrium condition achieved with 100 mg/L of P-CDP; α^H is the overall or summation solute hydrogen bond acidity; β^H is the overall or summation solute hydrogen bond basicity; π^H is a combined dipolarity/polarizability descriptor; R is the excess molar refraction; V is McGowan's characteristic volume in units of ($cm^3\,mol^{-1}/100$).

2.3.5.2 Selected data set

The $\log K_\infty$ values of 79 MPs were calculated using equation (5) and (6) and are reported in Appendix C. However, only 63 MPs had a C_e larger than the respective limit of quantification. A

total of 60 were randomly selected out of the 63 MPs for the LSER model training and verification. A random subset containing 40 values of K_{∞} were used as the training dataset to achieve the regression coefficients for the LSER model. Independent of the training data, the other 20 values of K_{∞} were used as a validation dataset to verify the prediction capability of the developed model.

2.3.5.3 Solvatochromic Descriptors

The solvatochromic descriptors (α^H, β^H, π^H, R, V) used to describe the properties of each individual MP were calculated with the software PaDEL-Descriptor developed by the National Singapore University[61] through a group contribution approach[62]. See Appendix C for the estimated values of each descriptor.

2.3.5.4 Multiple linear regression

Multiple linear regression (MLR) was performed to develop the equation between the solvatochromic descriptors and the affinity descriptor K_{∞} and to estimate the magnitude of the model coefficients. R Studio was used to fit equations and perform the analysis of variance (ANOVA). The regression model was evaluated by *p*-values. A *p*-value of the F test that was less than 0.01 indicates that at least one independent variable in the constructed model is useful in the prediction of K_{∞} at a 99% significant level. *p*-values less than 0.1 in ANOVA table indicated that the respective coefficients are non-zero at the 90% significant level. The part of the data set that can be explained by the parameters selected for this model was represented by the coefficient of determination (r^2). r^2 was also calculated for the validation data set to quantify the goodness-of-fit of the model predictions.

2.3.6 Analytical methods

Quantification of analytes from batch kinetics, instantaneous uptake, and affinity experiments was performed by high-performance liquid chromatography (HPLC) coupled with a quadrupole-orbitrap mass spectrometer (MS) (QExactive, ThermoFisher Scientific).

The analytical method was adopted from one previously reported for ultratrace level screening of polar and semi-polar organic chemicals[63] and involved HPLC-MS and on-line solid phase extraction (EQuan Max Plus, ThermoFisher Scientific). Samples were injected at 5 ml volumes and were loaded onto an XBridge (Waters) C-18 Intelligent Speed (2.1 mm × 20 mm, particle size 5 µm) trap column. Elution from the trap column and onto an XBridge (Waters) C-18 analytical column (2.1 mm × 50 mm, particle size 3.5 µm) was performed using a gradient pump delivering 200 µl min^{-1} of a water and MeOH mobile phase, each containing 0.1 vol.% formic acid. The HPLC-MS was operated with electrospray ionization in positive and negative polarity modes. The MS acquired full-scan MS data within a mass-to-charge range of 100–1,000 for each sample followed by a data-dependent acquisition of product ion spectra (MS/MS). Analytes were quantified from external calibration standards based on the analyte responses by linear least-squares regression. Limits of quantification for each analyte were determined as the lowest point in the external calibration curve at which at least 5 scans were measured across a chromatographic peak and the most intense MS/MS product ion was still detected. Exact molecular masses, ionization behavior, retention times, and limits of quantification used for the detection and quantification of each analyte are provided in Appendix A.

2.4 Results

Of the 90 MPs selected, only 83 of them were amenable to analysis by current analytical methods. The following sections describe the major results of the batch kinetics, instantaneous uptake, and affinity experiments for these 83 MPs. The raw data from the batch kinetics and instantaneous experiments are presented in Appendix D. The data from the affinity experiment and the LSER model development can be found in Appendix E.

2.4.1 Kinetics experiments

The kinetics of an adsorbent can be of great importance in the evaluation of adsorption efficiency, binding mechanism, and selectivity. To benchmark the kinetics of P-CDP against CCAC and achieve some insights into the potential of P-CDP in practical applications, two types of kinetics experiments have been performed including: (i) batch kinetics experiments; and (ii) instantaneous uptake experiments (filtration type).

2.4.1.1 Batch kinetics experiments

The purpose of the batch kinetics experiments was to evaluate the time required to reach equilibrium for adsorption of individual MPs by each adsorbent when the MPs are present in a complex mixture. Previous studies with CCAC and alternative adsorbents such as carbonaceous resin and high-silica zeolites show adsorption equilibrium is achieved in days to weeks and demonstrated that diffusion controlled transport contributes most to the slow kinetics of these adsorbents.[6,46,64] Through side-by-side comparisons between the kinetics of P-CDP and CCAC, the rate at which each MP reaches equilibrium adsorption on P-CDP and CCAC can be assessed and further insights can be gained into the specific adsorption mechanism of P-CDP. In addition, the batch kinetics of P-CDP is of great importance when it comes to potential applications. For

example, in adsorption followed by ultrafiltration (generally PAC-UF) processes, it has been demonstrated that the adsorption kinetics will impact the removal efficiency of MPs and treatment costs to great extents; faster kinetics will translate to reduced contact times, reduced reactor size, and less adsorbent required for a predetermined level of MP removal.[21,46] Further, in packed column filtration (generally GAC), it has been demonstrated that adsorption kinetics are negatively correlated with the rate of media replacement and the empty bed contact time (EBCT). In other words, faster adsorption kinetics can result in the generation of less waste of unsaturated adsorbent materials and a smaller reactor sizes or higher flow rates to attain a fixed level of MP removal.[18,19,65]

The rate at which the adsorption reaches equilibrium was described with the rate constant k_{obs} from the linear form of the Ho and McKay model[59] and showed that the adsorption kinetics are significantly faster for P-CDP than CCAC. The data in Figure 1 summarized the linearity of 4 representative MPs fitted with the Ho and McKay model. To show the complete story of the linearity of the MPs at different removal levels on P-CDP, the pseudo-second order models for famotidine (93.1% removed at equilibrium on P-CDP), isoproturon (67.8% removed), diclofenac (40.4% removed), and carbamazepine (18.0% removed) are provided in Figure 1. The great linearity for the data of these four MPs at different removal levels demonstrates that the adsorption kinetics of P-CDP can be described well with the Ho and McKay model.

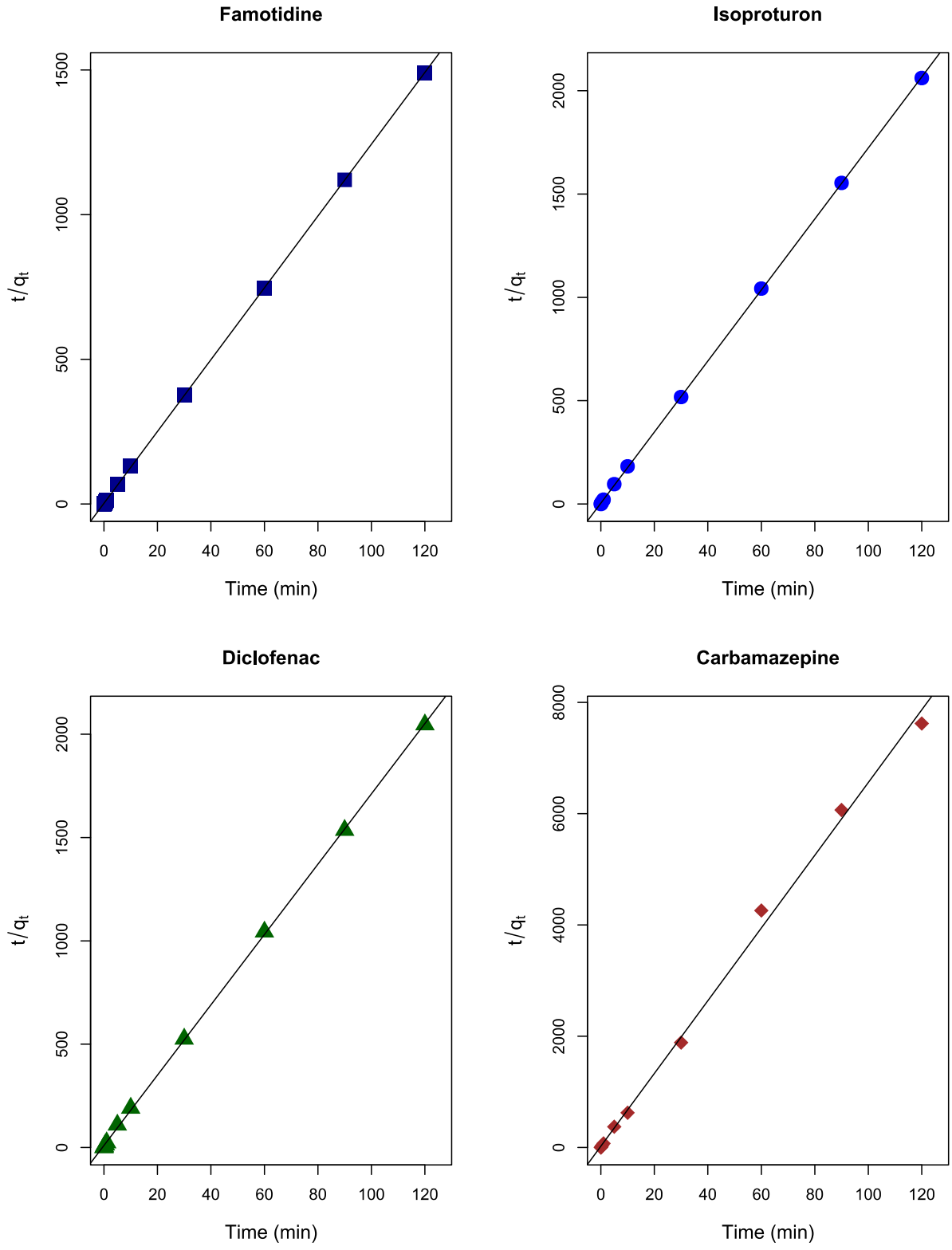

Figure 1. Pseudo-second order model of random representatives for 5-Group MPs onto P-CDP.

The estimated values of k_{obs} for each MP derived from the Ho and McKay model for CCAC and P-CDP are presented in the first two data columns in Table D1 of Appendix D. The data in Figure 2 summarize the distribution of the estimated values of k_{obs} for individual MPs for CCAC and P-CDP.

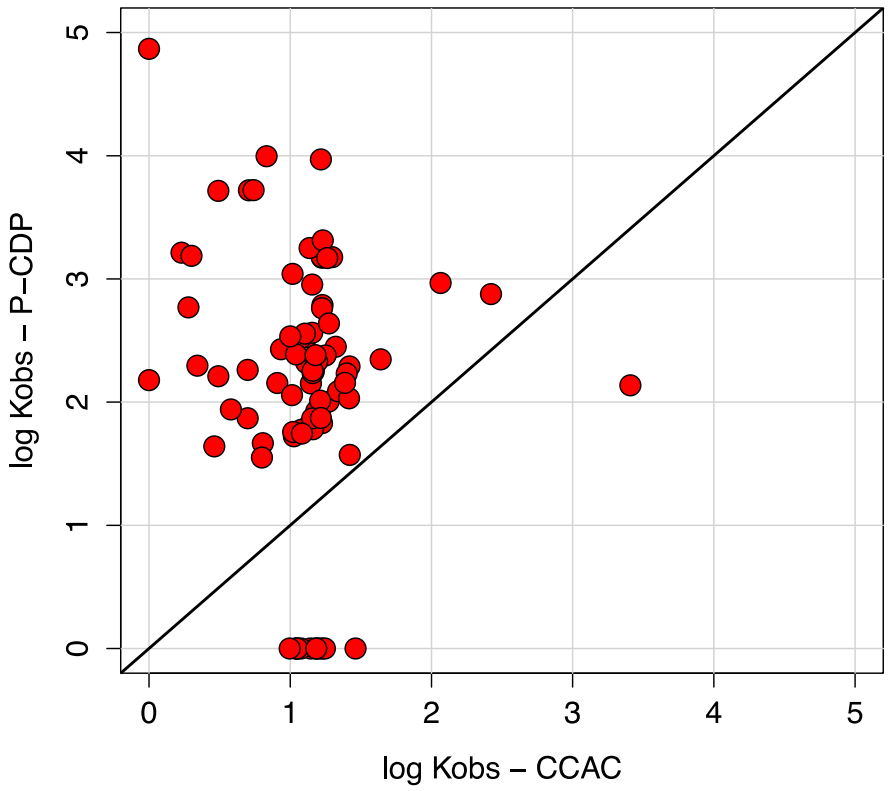

Figure 2. Distribution of $log\ k_{obs}$ estimated with Ho and McKay model for P-CDP and the CCAC

The values of k_{obs} from the Ho and McKay model for 70 of the 83 MPs are orders-of-magnitude larger for P-CDP than CCAC suggesting that the adsorption equilibrium of P-CDP can be achieved in a much shorter time. In other words, all available binding sites (i.e., β-CD monomers) on P-CDP are instantaneously accessible which is in accordance to the presumed complex-formation mechanism of β-CD. However, and very importantly, faster kinetics doesn't necessarily translate into a higher removal level of MPs at the adsorption equilibrium. As such,

the magnitude of k_{obs} for MPs that have little or no uptake can be misleading. For example, 2,4-D is hardly removed by P-CDP, yet the estimated value for k_{obs} is 72.9 g mg^{-1} min^{-1}. On the other hand, 2,4-D is removed fairly well by CCAC and the estimated value for k_{obs} is only 11.0 g mg^{-1} min^{-1}. The k_{obs} of 2,4-D is greater for P-CDP, but only because it rapidly reaches an equilibrium condition of no removal. Because of this, the k_{obs} for all MPs that are removed less than 5% are reported as zero in Figure 2 and Table D1 of Appendix D with the estimated value based on the Ho and McKay model given in parentheses. Two MPs were removed to less than 5% for CCAC and 12 MPs were removed to less than 5% for P-CDP, as presented in Figure 2.

To complement the estimated values for k_{obs} and to enable more robust interpretation of removal kinetics, the % removal of each MP after 5 minutes and 30 minutes for the CCAC and the P-CDP are provided in data columns 3 – 6 in Table D1 of Appendix D. These data provide insight into the extent of uptake at 5 minutes (early phase) and at 30 minutes (equilibrium point of P-CDP) for each adsorbent. Five groups of removal have been defined into which each MP could be binned: group 1 (G1) contains compounds with removal between 80 – 100%; group 2 (G2) contains compounds with removal between 60 – 80%; group 3 (G3) contains compounds with removal between 20 – 60%; group 4 (G4) contains compounds with removal between 5 – 20%; and group 5 (G5) contains compounds with no removal.

The data in Figure 3 summarize the batch removal of representative MPs from each of the removal groups on the P-CDP. Famotidine, isoproturon, diclofenac, carbamazepine, and 2,4-D were randomly selected to represent the removal kinetics of each of the five removal groups which indicate that the P-CDP adsorption equilibrium for MPs in all five groups can be reached within 10-30 mins, regardless of their final removal, compared to over 4 days for CCAC in this research (data not shown).

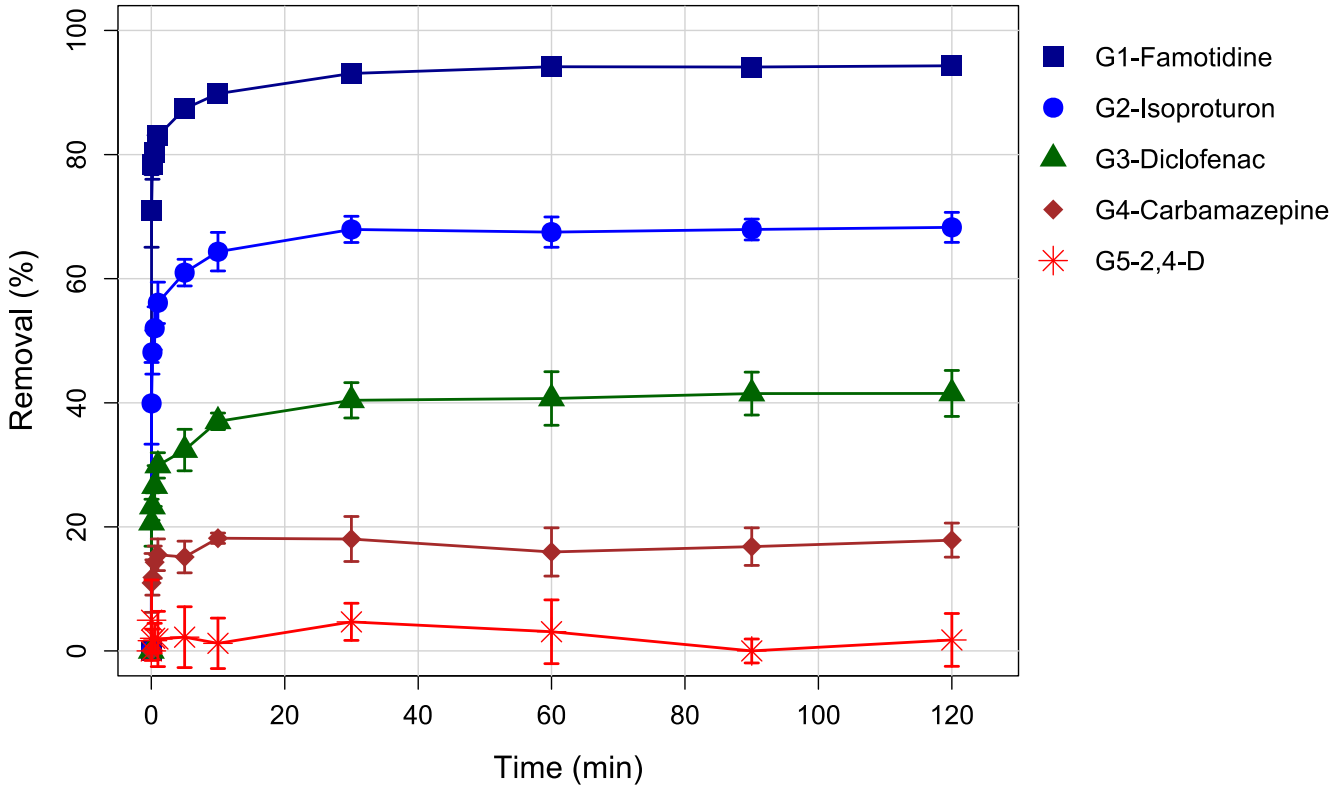

Figure 3. Adsorption kinetics of random representatives for 5-Group MPs onto P-CDP. Error bars represent standard deviations of 5 replicates.

The data presented in Table 2 summarize the distribution of the 83 MPs in each of the five defined removal groups after 5 minutes and 30 minutes of contact time for each adsorbent. There are two important observations to note with respect to these data. First, 19 MPs attained greater than 80% removal (Group 1) in 5 minutes for P-CDP whereas only 3 MPs attained that level of removal in 5 minutes for CCAC. This shows that the P-CDP can nearly completely remove some MPs from water at rates that exceed the capabilities of CCAC. This observation speaks to an apparent affinity or selectivity of the P-CDP towards some types of MPs. Second, the distribution of MPs in each removal group did not change much for P-CDP from 5 minutes to 30 minutes. However, due to slower equilibrium kinetics, the distribution of MPs in each of the removal groups skewed strongly towards greater removal after 30 minutes for the CCAC. This

observation speaks to the relative capacities of each of the adsorbents. As presented in Appendix B, the Brunauer-Emmett-Teller (BET) surface area of CCAC is 1085 m^2/g which is about 5 times larger than that of P-CDP (218 m^2/g). Therefore, the available binding sites on CCAC should be more than the available binding sites on P-CDP. As a result, MP removal on CCAC is slow but non-selective and has a high capacity for MP adsorption.

Table 2. Distribution of MPs in each of 5 Groups at 5 minutes and 30 minutes for P-CDP and CCAC

Adsorbent	**P-CDP**		**CCAC**	
Times	**5 minutes**	**30 minutes**	**5 minutes**	**30 minutes**
Group 1	19	23	3	38
Group 2	13	14	13	28
Group 3	17	16	60	15
Group 4	23	18	5	0
Group 5	11	12	2	2

In addition to the faster kinetics and lower capacity, the apparent selectivity of adsorption onto P-CDP is particularly interesting. As presented in Appendix D, there are eleven MPs that are not effectively removed by CCAC that are removed well by P-CDP: albuterol, amphetamine, atenolol, atenolol acid, codeine, hydrocodone, morphine, nadolol, prometon, tramadol, and venlafaxine. Interestingly, among these eleven MPs, ten are positively charged at neutral pH. Their good removal by P-CDP could be contributed to the unique uptake mechanism. β-CD encapsulates compounds to form well-defined host-guest complexes and it has been demonstrated in previous studies that the non-bonding electron pairs of the glycosidic oxygen bridges are directed toward the inside of the cavity of β-CD producing high electronegativity.[55] In contrast, among 23 MPs containing negative charges, the removal of 17 are less than 50 % for P-CDP and the removal of 22 are higher for CCAC than for P-CDP at 30 minutes. It should be noted that 30 minutes is far from enough time for CCAC to achieve equilibrium which indicates that the removal of these 22 MPs could be even higher for CCAC. Considering these results and

the electrostatic interactions, it is sensible to generate a hypothesis that the P-CDP favors the adsorption of MPs with positive charges and cannot effectively remove some MPs with negative charges due to the high electronegativity of the cavity of β-CD.

In sum, compared with CCAC, the P-CDP has faster kinetics, lower capacity and higher selectivity for MPs in batch adsorption. Further, the selectivity of P-CDP presented in batch kinetics experiments leads to the hypothesis that the P-CDP favors the adsorption of MPs with positive charges and cannot effectively remove MPs with negative charges due to the electrostatic interactions.

2.4.1.2 Instantaneous uptake experiments

The purpose of the instantaneous uptake experiments was to simulate filtration-type treatment processes. From the results of batch kinetics experiments, the fact that the adsorption equilibrium of P-CDP can be achieved in minutes reveals some potential advantages of P-CDP in the application of filtration-type treatment processes including the generation of less waste of unsaturated adsorbent materials and smaller reactor sizes or higher flow rates to attain a fixed level of MP removal.[18,19,65] Further insights can be gained into the potential for P-CDP to be used in packed column filtration through side-by-side comparisons between the instantaneous uptake of MPs by P-CDP and CCAC. Though a complete breakthrough curve and throughput in bed volumes[19] can't be evaluated with this type of simulation, instantaneous experiments can be used to predict the performance of P-CDP based on the comparison with CCAC, a common and well investigated adsorbent in packed column filtration.[18,51,66]

The removal of 83 MPs on P-CDP and CCAC with short contact time was assessed through the instantaneous uptake experiments and indicated that the P-CDP can adsorb more MPs to greater extents with flow-through conditions (i.e., short contact time) compared with CCAC. The

data in Figure 4 summarize the instantaneous removal of the 83 MPs on P-CDP and CCAC. The results of instantaneous uptake experiments are also presented columns 7 – 8 in Table D1 in Appendix D.

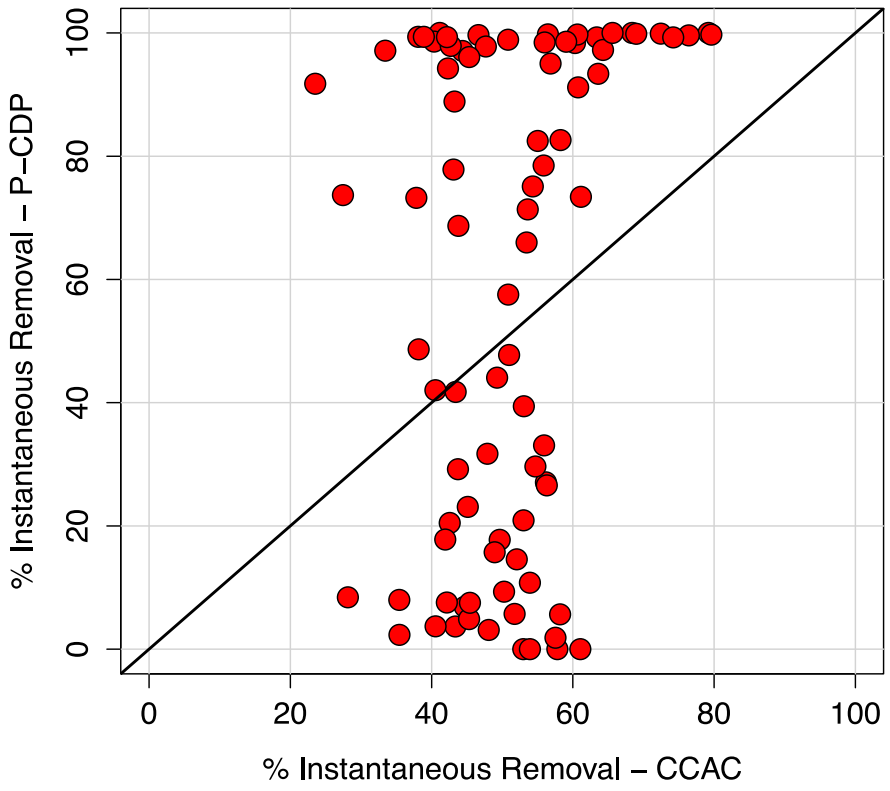

Figure 4. Distribution of instantaneous removal of 83 MPs by P-CDP and CCAC

As presented in Figure 4, a total of 47 MPs had greater instantaneous uptake on P-CDP than on CCAC. Interestingly, 35 MPs had instantaneous removal of greater than 80% on P-CDP (31 of the MPs were greater than 90%) whereas only 23 MPs were identified in G1 for P-CDP after 5 minutes. The additional 12 MPs removed over 80% during instantaneous uptake experiments were all G2 MPs in batch kinetics experiments indicating that the filtration-type treatment could be better than the batch treatment for P-CDP, perhaps due to the complete contact between the chemical mixture and the P-CDP in filtration. However, it can also be attributed to the fact that

the ratio of P-CDP to the chemical mixture (0.3 mg for 8 ml mixture) during instantaneous experiments is about 4 times higher than the ratio of P-CDP to the chemical mixture (1 mg for 100 mixture) during the kinetics experiments. Considering all binding sites on P-CDP are instantaneously available, it is sensible that the removal levels of MPs are improved in filtration-type experiments. There were also 14 MPs that were removed to less than 10% for P-CDP; all of these MPs were previously classified as G4 or G5 MPs in the batch kinetics experiments. In contrast, no MPs had instantaneous removal greater than 80% for the CCAC; all MPs were removed between 20 – 80% aligning well with the previous classification defined for the batch kinetics experiments after 5 minutes of contact time. As previously observed in the results of batch kinetic experiments, the instantaneous removal of 83 MPs by P-CDP was distributed over a broader range compared with CCAC indicating that the P-CDP is more selective on the adsorption of MPs than the CCAC.

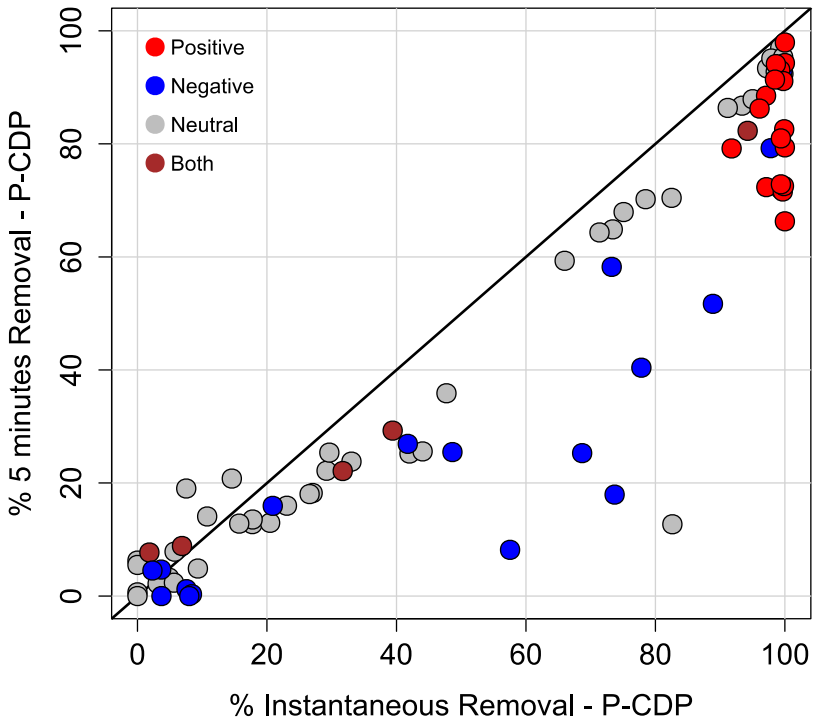

Figure 5. Distribution of 5 minute batch removal and instantaneous uptake of 83 MPs by P-CDP. Compounds with positive charges are marked as red; Compounds with negative charges are marked as blue; Compounds with no charge are marked as grey and zwitterions are marked as brown.

The data in Figure 5 summarize the 5 minute removal in batch and the instantaneous uptake in filtration-type experiments. Clearly the removal level of nearly all the MPs are higher for the instantaneous uptake than the batch kinetics experiments which could be contributed to the complete contact between the chemical mixture and the polymer in filtration or the higher ratio of P-CDP to the chemical mixture as stated previously. Further, the positive correlation between the 5 minute batch removal and the instantaneous uptake of MPs on P-CDP indicates that the removal level of each MP in filtration aligns well with the removal of the respective MP in batch. For example, from the clusters of red points on the top-right area and blue points on the bottom-left area of Figure 5, it can be confirmed that the positively charged MPs were removed effectively and the negatively charged MPs were not removed well by P-CDP both in batch and filtration-type experiments. It should be noted, however, that several negatively charged MPs are

removed to an intermediate level, which indicates that there are some other important physicochemical properties which impact the adsorption of P-CDP besides the charge state.

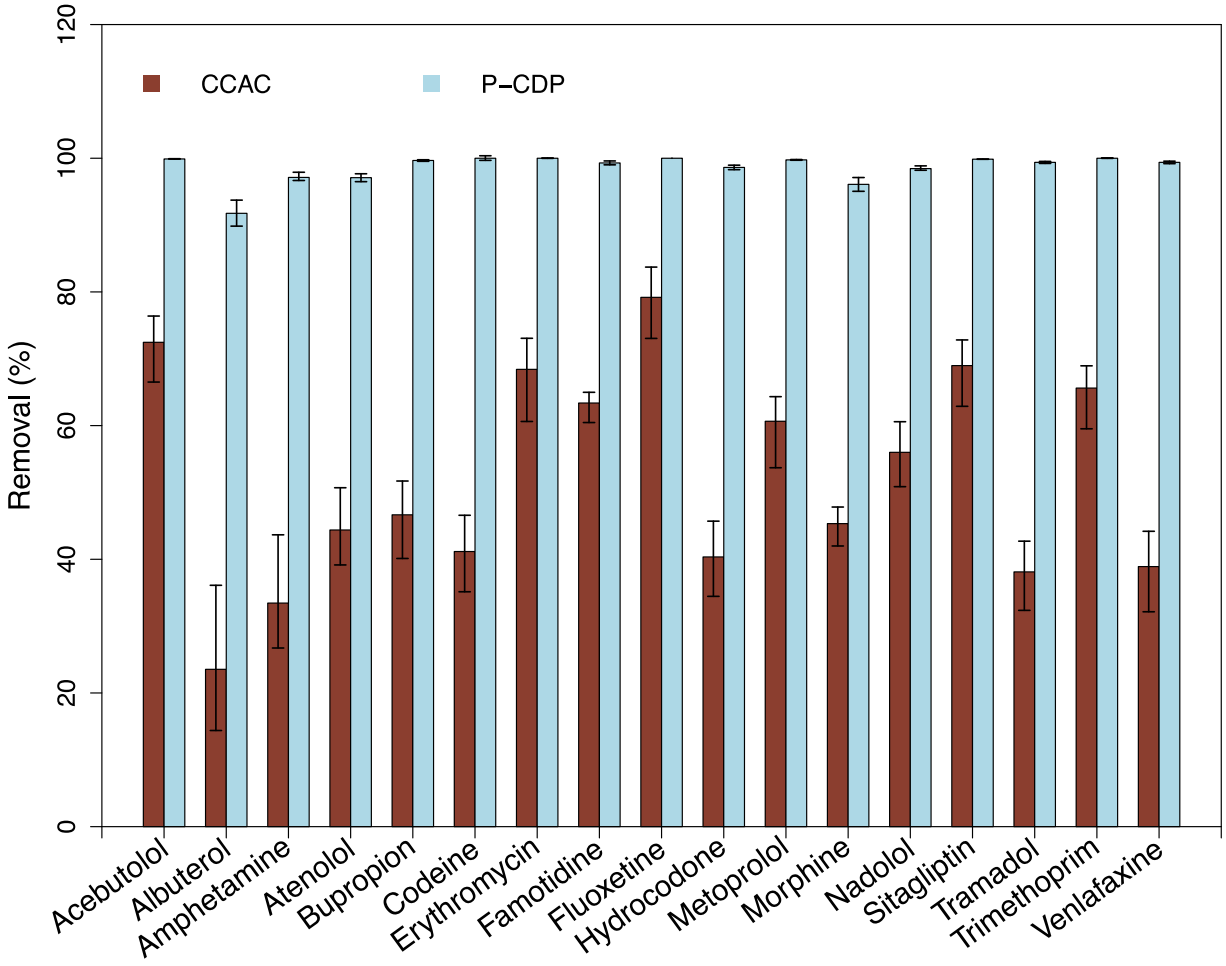

Figure 6. Instantaneous removal of 17 positively charged MPs by CCAC and P-CDP. Error bars represent maximum and minimum removal of triplicates.

The data in Figure 6 summarize the instantaneous removal of 17 positively charged MPs by P-CDP and CCAC which is a guide to the eye to present the high efficiency of P-CDP in the adsorption of cations. All 17 positively charged compounds not effectively removed by CCAC show almost complete removal on P-CDP in the instantaneous uptake experiments. Therefore, the previous hypothesis that the P-CDP favors the adsorption of MPs with positive charges due to the electrostatic interactions can be verified with the similar results of instantaneous uptake experiments.

In sum, compared with CCAC, the P-CDP has faster kinetics and higher selectivity for MPs in filtration-type adsorption processes. In addition, the observation that the removal level of most MPs are higher in instantaneous uptake than in batch experiments could be contributed to the complete contact between the chemical mixture and the P-CDP in filtration or the higher ratio of adsorbent to adsorbates in filtration-type experiments. Further, the great removal efficiency of P-CDP presented in instantaneous experiments for all 17 positively charged MPs confirm the hypothesis that the P-CDP favors the adsorption of MPs with positive charges due to electrostatic interactions. However, the comparatively high removal of several negatively charged MPs indicates that there should be some other important physicochemical properties which impact the adsorption of P-CDP besides the charge state.

2.4.2 Affinity experiments

The purpose of the affinity experiments was to characterize the affinity of different MPs to the P-CDP and to support the development of an LSER that can explain the selectivity of the P-CDP. In the previous sections, the P-CDP presents an orders-of-magnitude faster kinetics and much greater instantaneous removal as compared with CCAC, however, MP adsorption efficiency by P-CDP was also distributed over a broader range than CCAC indicating that the P-CDP is more selective than CCAC. The selectivity of an adsorbent can be of great importance when it comes to the understanding of the adsorption mechanism and the evaluation of its potential in practical applications. To describe the selectivity of P-CDP for each MP, the distribution coefficient of each MP at infinite dilution (K_∞), which was proposed in previous studies about the adsorption of AC as the best descriptor for the affinity,[60,62,67,68] was estimated from experimental data. The values of K_∞ have been calculated for 63 of the 83 MPs for which C_e was larger than the respective limit of quantification and are reported in Table C1 of Appendix C.

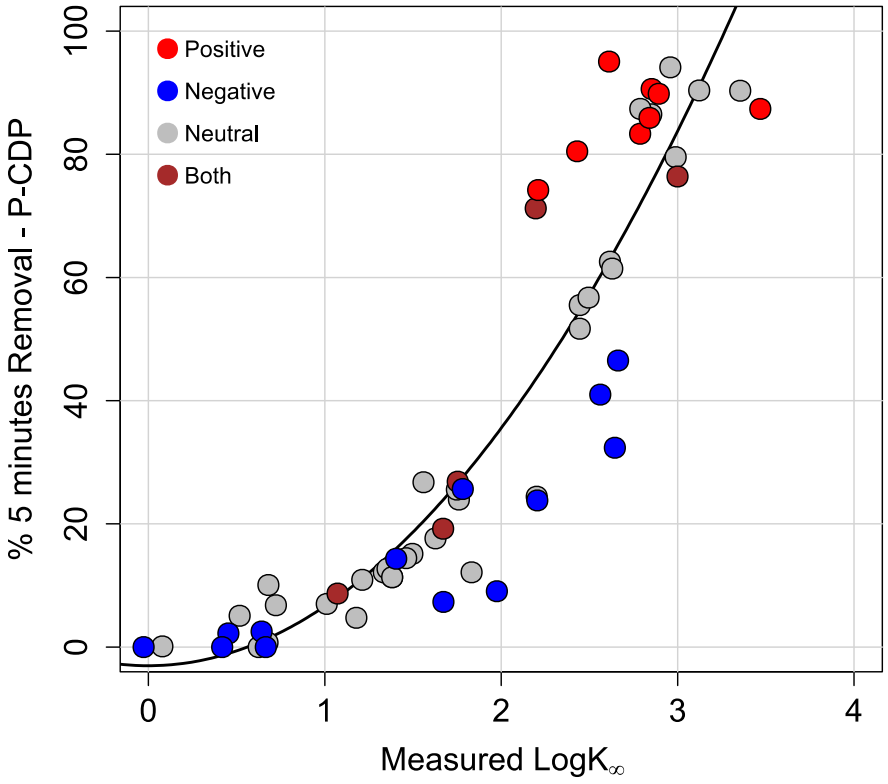

Figure 7. Distribution of 5 minute batch removal and calculated $log\ K_\infty$ for 60 MPs for P-CDP. Compounds with positive charges are marked as red; Compounds with negative charges are marked as blue; Compounds with no charge are marked as grey and zwitterions are marked as brown.

The data presented in Figure 7 summarize the 5 minute removal and the estimated value of $\log K_\infty$ of the 60 MPs. The positive correlation between 5 minute removal and the values of $\log K_\infty$ for each MP demonstrates that the greater the affinity of a MP to the P-CDP is, the higher the removal level of this MP for P-CDP will be. For example, among the 60 MPs, all 8 positively charged MPs which show great removal by P-CDP in batch kinetics and instantaneous uptake experiments also present the highest values of affinity. Further, 9 of the 12 negatively charged compounds which show poor removal by P-CDP in the previous sections also present the comparatively low values of affinity. Therefore, the hypothesis generated previously that the P-CDP favors the adsorption of MPs with positive charges due to the electrostatic interactions can also be well supported with the calculated values of K_∞ from the affinity experiments. In

addition, two important observations: (i) several negatively charged MPs show comparatively high K_∞; and (ii) the K_∞ of non-charged MPs and zwitterions distribute evenly in Figure 7, support the hypothesis generated in previous sections that there are some other important physicochemical properties which impact the adsorption of P-CDP besides the charge state. Importantly, the values of $\log K_\infty$ for each MP for P-CDP spread out over four orders of magnitude indicating the selectivity of P-CDP observed in the kinetics experiments.

2.4.3 Linear Solvation Energy Relationship

Though the selectivity/affinity of P-CDP for different MPs is important for getting deeper insight into the potential and properties of P-CDP, it is not practical to perform adsorption experiments on all types of MPs.[1,5] To target the selectivity of P-CDP rising from the results of kinetics, instantaneous uptake, and affinity experiments, a specific form of LSER was adopted to conduct the prediction of the affinity of different MPs to P-CDP. Among the 5 specific solvatochromic descriptors (α^H, β^H, π^H, R, V) used in this model, none of them can be directly linked with the charge state of MPs. As a result, the charge-state hypothesis generated in previous sections cannot be verified trough the statistical analysis of the LSER model. The calculated values of $\log K_\infty$ and solvatochromic descriptors for all 60 MPs are presented in columns 1 – 6 in Table C1 presented in Appendix C. The distribution of solvatochromic descriptors (α^H, β^H, π^H, R, V) for both the training dataset and validation dataset were also presented in Figure 8 with a box and whisker plot. The distribution of each descriptor in the validation dataset matches that in the training dataset indicating that the validation dataset will be a great representative to verify the model developed with the training dataset.

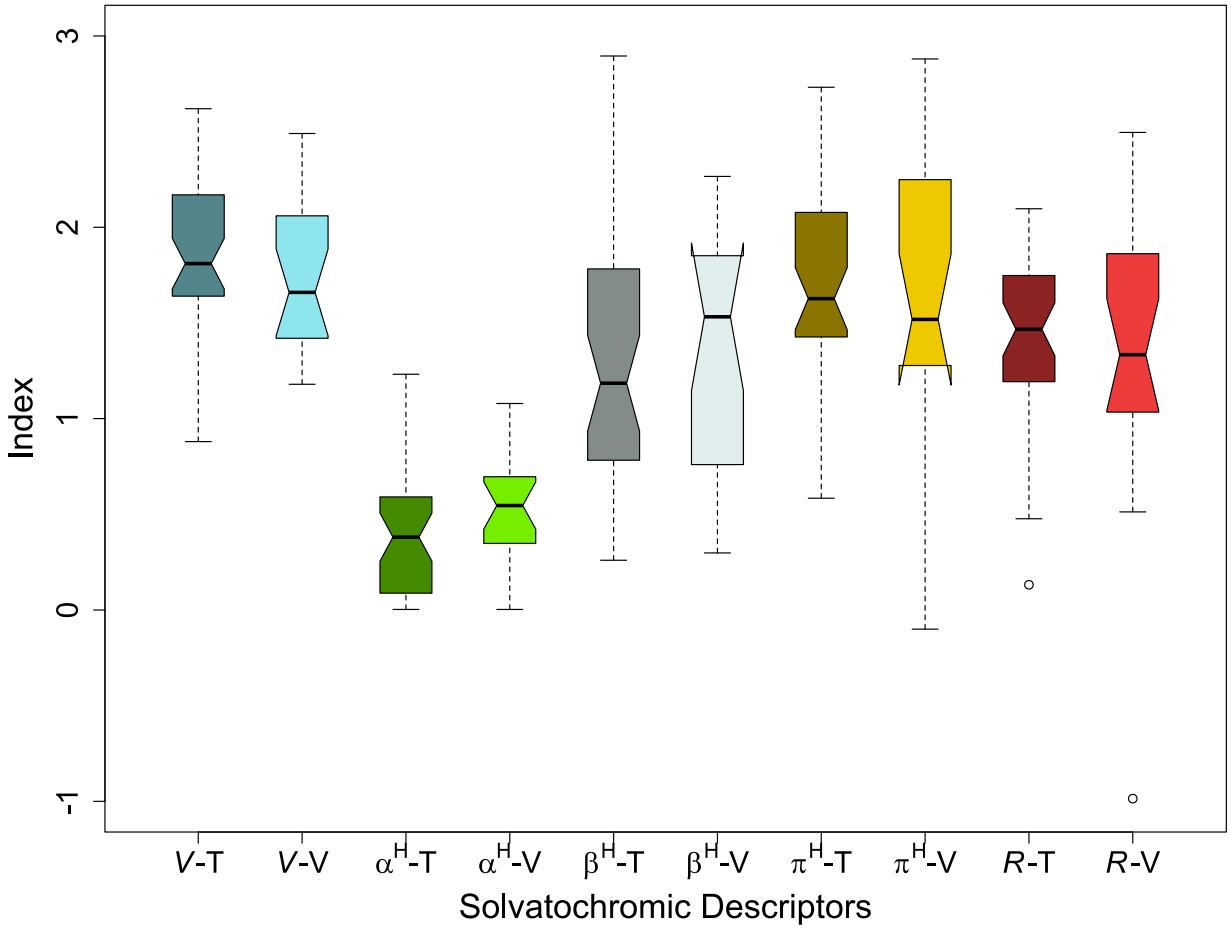

Figure 8. Box and whisker plot for the distribution of solvatochromic descriptors. Descriptors for training dataset of 40 MPs are ended with (-T) and those for validation dataset of 20 MPs are ended with (-V).

2.4.3.1 Development of the LSER model

The coefficients of the LSER descriptors were determined with MLR between the independent variables (LSER descriptors) and dependent variables ($\log K_{\infty}$). The details of MLR and ANOVA analysis can be found in Table E1 to Table E4 presented in Appendix E. The equation generated with the training dataset is presented as follows:

$$\log K_{\infty} = -(2.96 \pm 0.48) + (0.41 \pm 0.27)\alpha^H + (0.01 \pm 0.14)\beta^H$$

$$+(0.18 \pm 0.23)\pi^H + (0.26 \pm 0.21)R + (2.15 \pm 0.22)V$$

$$(n = 40, r^2 = 0.79) \quad (9)$$

The *p*-value of the F test for this MLR model was 1.5e-10 indicating that this model can be useful in the prediction of K_{∞} at a significance level much higher than 99%. In other words, at least one of the 5 descriptors is very important in the prediction of affinity of MPs onto P-CDP. Further, the magnitude of the coefficient of the *V* term was much higher than the coefficients of the other terms indicating that the McGowan's characteristic volume was the most influential descriptor in the LSER model for P-CDP and contributed the most to the goodness-of-fit of this model (r^2). The large and positive value of the coefficient for *V* indicates that within the specific range of McGowan volume from 0.87 to 5.73 ($cm^3\,mol^{-1}/100$) in this case, MPs with large volumes tend to have higher affinity to P-CDP, though it is possible that MPs with large volumes will not bind to P-CDP due to other physicochemical properties such as negative charges that do not favor binding to P-CDP. The tendency of P-CDP to adsorb MPs with large volumes could be contributed to two facts: (i) the large molar volume of MP could thermodynamically drive the adsorption because it requires more energy for cavity formation in water for larger molecules; or (ii) it is demonstrated in some previous projects that adsorption by β-CD is based on the size-matched host-guest chemistry[22,52,55] indicting that the molar volume of adsorbates could essentially determine the adsorption onto P-CDP. In contrast, the small magnitude and large *p*-value of the other 4 coefficients suggest that the hydrogen bond formation (α^H and β^H), polarizability (π^H), and the molecular force of lone-pair electrons (*R*)[67] only played a minor role in this model compared with volume. Since β^H is insignificant at any reasonable statistical level

based on the ANOVA test, it is possible that a better model with fewer independent descriptors could be achieved by excluding the descriptor β^H from the full model.

As a result, a reduced model with only four independent descriptors (α^H, π^H, R, V) was generated with the same training data set. The equation is presented as follows:

$$\log K_{\infty} = -(2.96 \pm 0.47) + (0.41 \pm 0.27)\alpha^H + (0.20 \pm 0.17)\pi^H$$

$$+(0.25 \pm 0.20)R + (2.15 \pm 0.21)V$$

$$(n = 20, r^2 = 0.79) \quad (10)$$

The *p*-value of the F test for this model was 2.5e-11 which is smaller than the *p*-value of the full model indicating that the significance of the reduced model was improved by excluding the term β^H compared with the full model. Further, the ANOVA test between the full and reduced model demonstrated that at over a 90% significance level as presented in Table E4 in Appendix E, the existence of the term β^H made no statistical difference on the LSER model for P-CDP. As a result, the LSER between MPs and P-CDP in aqueous solution can be described with a subset of solvatochromic descriptors with α^H, π^H, R and V**.** The developed model can be used to predict the affinity of other organic chemicals to the P-CDP based on the estimated values of these four solvatochromic descriptors.

2.4.3.2 Verification of the LSER model

As shown in Figure 8, the ranges of solvatochromic descriptors for the validation dataset are in accordance to the ranges of training dataset indicating that the validation dataset can be representative for the verification of the LSER model developed with the training dataset. The

predicted $\log K_\infty$ values obtained from Equation (9) were plotted against the experimental $\log K_\infty$ for both datasets in Figure 9.

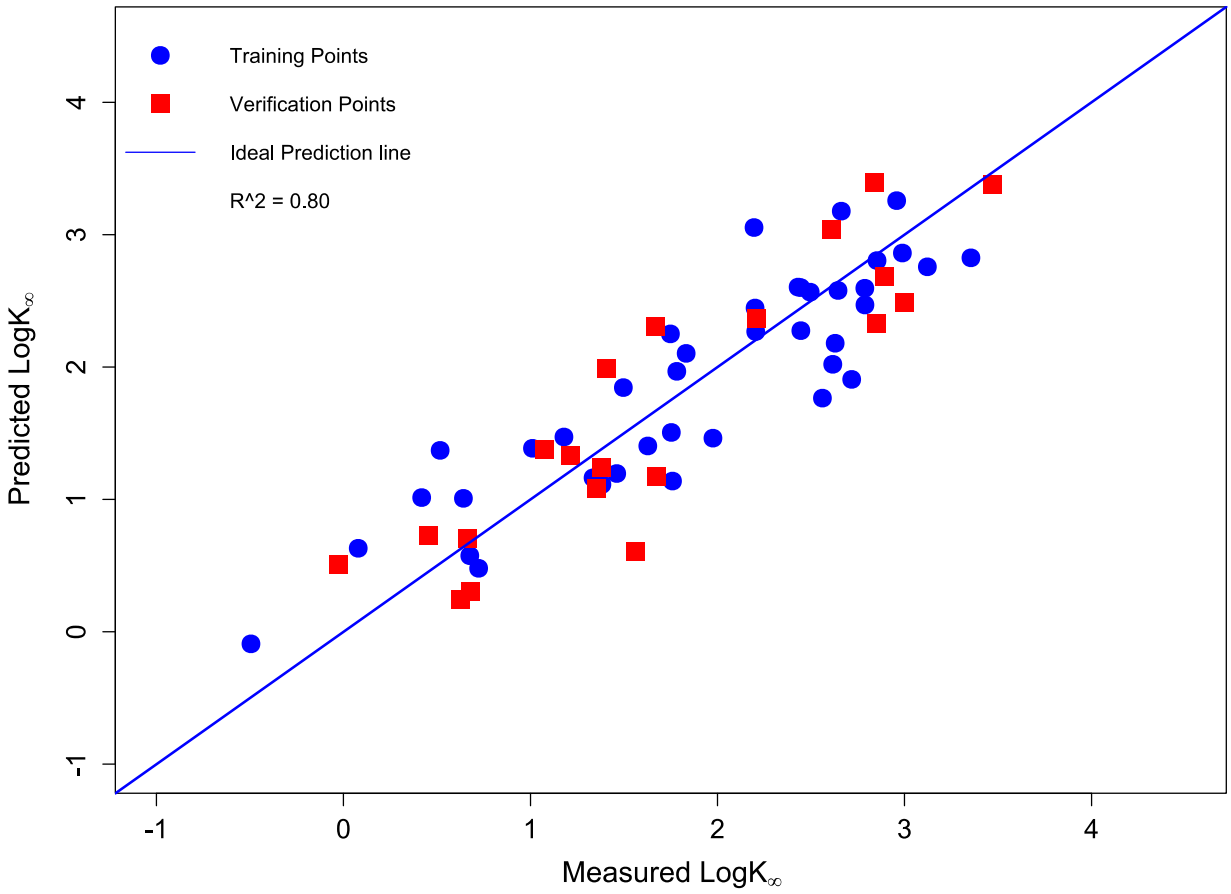

Figure 9. The predicted affinity descriptors vs experimentally measured affinity descriptors by full model (Equation 9) for both training and validation data sets.

The predicted $\log K_\infty$ values obtained from Equation (10) were plotted against the experimental $\log K_\infty$ for both datasets in Figure 10.

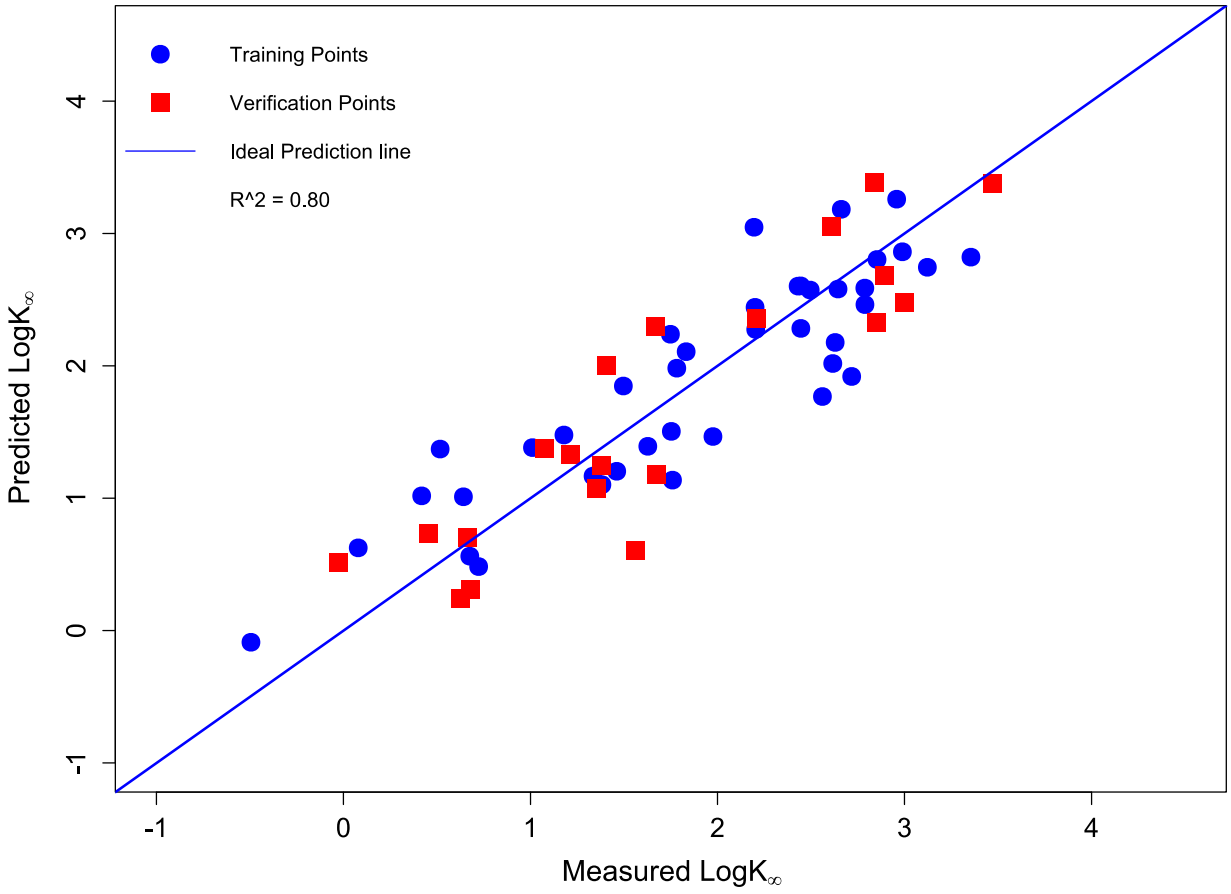

Figure 10. The predicted affinity descriptors vs experimentally measured affinity descriptors by reduced model (Equation 10) for both training and validation data sets.

Validation of the full and reduced models was conducted with 20 validation compounds as presented in Table C1 in Appendix C. The goodness-of-fit was quantified with the coefficient of determination (r^2). The r^2 of the validation with both models are both around 80%, suggesting satisfactory prediction capabilities of the full and reduced LSER models. Further, the higher *p*-value and same value of r^2 for the reduced model indicates that the prediction capabilities of the reduced model are at least the same as that of the full model if not better. Therefore, The LSER model with four independent descriptors (α^H, π^H, R, V) could perform a satisfactory prediction of the affinity to P-CDP and serve as a guide for the application of P-CDP in practical water or

wastewater treatment processes including adsorption followed by ultrafiltration and packed column filtration.

Importantly, besides the charge-state hypothesis generated in previous sections, the LSER model demonstrates that molecular volume (*V*) is another physicochemical property that can influence the adsorption of MPs onto P-CDP to great extents. As proven in previous studies, β-CD can only encapsulate size-matched guest compounds (<20 Å) due to the limited size of the cavity of β-CD. [52,55,58,69] Further, most MPs fall into the diameter range of 6 to 10 Å and the majority of NOM molecules are larger than 20 Å.[6,18] Through the statistical analysis of the LSER model, further understanding has been gained into the size-matched mechanism for P-CDP that in the diameter range from 6 to 10 Å (i.e., McGowan volume from 0.87 to 5.73), the affinity of P-CDP is positively correlated with the diameter of the MPs. Additionally, though the charge-state hypothesis cannot be directly verified through the developed model, further insights can be achieved by looking into the molecular volume of all 8 positively charged MPs adopted in this model. The McGowan volume of these 8 MPs range from 1.98 to 2.49 ($cm^3\,mol^{-1}/100$) which is the intermediate of the full range from 0.87 to 5.73 in this case. However, all these MPs have the highest distribution coefficients in the affinity experiments indicating that the positive charges of MPs (McGowan volume range from 0.87 to 5.73) can determine the complex formation on P-CDP.

As a result, a new hypothesis can be generated based on the support from the LSER model that the P-CDP favors the adsorption of MPs large in size but the charge state (positive charge) of MPs can determine the inclusion in the specific range of McGowan volume from 0.87 to 5.73 ($cm^3\,mol^{-1}/100$).

CHAPTER 3: DISCUSSION AND FUTURE WORK

3.1 Discussion

Through the batch kinetics, instantaneous uptake, and affinity experiments, the performance of P-CDP was characterized for the removal of 83 MPs from water at environmentally relevant concentrations and its performance was benchmarked against CCAC. Two important hypotheses of the charge states and the McGowan volume about the adsorption mechanism of P-CDP have been generated based on the consistent observations throughout the three sets of experiments. Some interesting features of P-CDPs were also observed during the analysis of the resulting data by which the potential of P-CDP to be used in practical water and wastewater treatment processes can be evaluated.

First, the relatively fast kinetics (i.e., quick equilibrium) has been demonstrated in both batch and filtration-type kinetics experiments suggesting that all available binding sites on P-CDP can be instantaneously accessed. As proven in previous studies, the adsorption of β-CD is based on the complex-formation mechanism[52,55] which is much more specific and efficient than the diffusion controlled adsorption on AC. Therefore, it is sensible that the kinetics of P-CDP, which also has high surface area and porosity, can be much faster than that of AC.

Second, it has been observed in batch kinetics, instantaneous uptake, and affinity experiments that the adsorption of P-CDP can be impacted by some certain physicochemical properties of MPs (i.e., the adsorption is selective). For example, positively charged MPs (i.e., cations) can be efficiently removed by P-CDP which could be contributed to the electrostatic interactions between the cations and the high electronegativity inside the cavity of β-CD.[55] Importantly, the cations were not effectively removed by CCAC indicating the potential of P-CDP as an alternative adsorbent to make up for this deficiency of AC.

Third, the statistical analysis of the LSER model demonstrates that the molecular volume of a MP is of great importance for its adsorption by P-CDP. The large and positive value of the coefficient for *V* in the LSER model indicates that within the specific range of McGowan volume from 0.87 to 5.73 ($cm^3\ mol^{-1}/100$), MPs with large volumes tend to have higher affinity to P-CDP but the positive charges can determine the complex formation even for MPs with comparatively small volumes and it is possible that MPs with large volumes will not bind to P-CDP due to other physicochemical properties such as negative charges that do not favor binding to P-CDP.
Last but not least, the results of batch kinetics, instantaneous uptake, and affinity experiments align well with each other which is important for extrapolating results attained in one type of process to another. Further, due to the positive correlation between the removal level (batch or filtration) and the affinity of MPs for P-CDP, the removal efficiency of a MP during either type of treatments can be well estimated with the respective affinity to P-CDP which can be predicted by the LSER model with no need for any experiments.

In practice, the P-CDP can be an alternative adsorbent to be used in practical treatment processes combining its fast kinetics and great affinity for cations that are poorly removed by AC. For example, PAC-UF, suggested as the most suitable treatment for sensitive receiving waters,[21] can be an efficient way to remove MPs. However, the slow kinetics (i.e., small k_{obs}) of PAC results in typically required PAC-UF contact times of 0.5-2 h[23,56] which are still too short for PAC to reach adsorption equilibrium and thus do not take full advantage of the capacity of PAC. A recent study on SPAC demonstrates the improvement in kinetics by wet milling PAC to SPAC with a final d_{50} of 1 μm but it also proves that SPAC suffers more severe blocking effects caused by NOM than PAC.[46] The P-CDP, as a potential alternative for PAC-UF, presents a much faster kinetics compared with CCAC and other widely used PAC. Though the time to

equilibrium for adsorption of SPAC is significantly shortened, the additional step of wet milling PAC to SPAC will significantly increase the cost of energy and money. Considering the intensive energy consumption in the production of SPAC, the P-CDP will be a better choice when it comes to the sustainable water and wastewater treatment.

As another important application, packed column filtration has been demonstrated to have potential for the control of MPs and has been applied in some water or wastewater treatment plants. However, the slow kinetics of GAC results in the gradual breakthrough curve and long EBCT. Importantly, the performance of GAC in packed columns can also be adversely affected by the presence of NOM and DOC in natural water or wastewater.[17,70,71] Due to the competition and pore-blockage mechanism by NOM demonstrated in previous studies[72–74], the adsorptive capacity of GAC can be significantly reduced. Further, NOM adsorption can decrease the kinetics of GAC by reducing MP adsorption rates.[39] As a result, the breakthrough curve of GAC can be severely influenced by NOM in water and longer EBCT has to be selected to reach the predetermined removal level of MPs accordingly. It should be noted, in addition, much GAC can be wasted because of the large mass transfer zone caused by the gradual breakthrough curve which will increase the media replacement cost.[65]

Compared with GAC, the much faster kinetics of P-CDP suggests that the breakthrough curve of P-CDP in a packed column could be much steeper than that of GAC (like ion exchange) resulting in a much smaller mass transfer zone. Further, as demonstrated in previous studies, β-CD can only encapsulate size-matched guest compounds (<20 Å)[52,55,58,69] indicating that the adsorption of MPs by β-CD polymers will not be severely interfered by natural water constituents including NOM and salinity due to molecular recognition. For example, similar removal efficiencies for MPs were observed in deionized water and lake water for β-CD

polymers (β-CD polyurethanes and EPI-CDP) in previous studies[22,75] which can support the potential non-interference property of P-CDP. Therefore, it is possible that the performance of P-CDP in filtration type treatments won't be adversely affected by the presence of NOM and DOC in natural water or wastewater.

Together, data from the batch kinetics, instantaneous uptake, affinity experiments and the LSER model provide key insights into the mechanisms by which MPs bind to the P-CDP and demonstrate its adsorption efficacy relative to AC. Though the adsorption of MPs is more selective for P-CDP than CCAC, potential advantages including the fast kinetics, efficient removal of cations and non-interference by NOM suggest that the P-CDP could be a suitable alternative to activated carbon with potential applications in water purification and wastewater treatment.

3.2 Conclusions

- P-CDP shows much faster kinetics than CCAC and reaches adsorption equilibrium nearly instantly, suggesting instantaneous accessibility of all binding sites which can be contributed to the complex-formation mechanism of P-CDP in contrast to the diffusion controlled adsorption of CCAC.

- The extent of overall removal of MPs is lower for P-CDP compared to an equivalent mass of CCAC, suggesting that CCAC has greater adsorption capacity on a per mass basis which can be contributed to the 5 times higher surface area of CCAC as compared with P-CDP.

- The rate constant k_{obs} and extent of removal of different MPs are narrowly distributed for CCAC, confirming non-selective adsorption. Conversely, the broad range of rate constants and removal extents of different MPs for P-CDP suggests selective adsorption.

- The charge state of MPs can impact the adsorption of P-CDP to great extent especially for the cations. P-CDP can rapidly and efficiently remove cationic species under both batch and filtration adsorption which are not well removed by CCAC.

- The positive correlation between 5 minute removal and the values of $\log K_{\infty}$ for each MP demonstrates that the removal efficiency of a specific MP onto P-CDP can be estimated based on the value of distribution coefficient which can be well predicted with the LSER model.

- The LSER model suggests that McGowan's volume serves as a major determinant of MP uptake by P-CDP. Within the specific range of McGowan volume from 0.87 to 5.73 (cm^3 mol^{-1}/100), MPs with large volumes tend to have higher affinity to P-CDP but the charge

state (positive charges) of MPs can determine the inclusion even for MPs with comparatively small volumes.

- Potential advantages including the fast kinetics, efficient removal of cations, and expected non-interference by NOM suggest that the P-CDP could be a suitable alternative to AC with potential applications like batch adsorption contactor processes followed by ultrafiltration or filtration-type column treatment.

3.2 Future work

All of the data presented in this thesis demonstrate that the P-CDP can instantaneously remove MPs with certain physicochemical properties from water. From these data, two important properties, including the charge state and molecular volume have been confirmed to impact the adsorption onto P-CDP to great extents. Further, the apparent importance of molecular volume demonstrated by the LSER model and previous studies also suggests that large molecules such as most NOM and DOC will be excluded from the adsorption of P-CDP. Therefore, natural water constituents, which are major causes of the fouling problem for non-selective adsorbents such as AC, might not interfere the adsorption of P-CDP. Additionally, the regeneration of P-CDP was achieved with a methanol rinse at ambient temperatures with no reduced performance in a previous study suggesting the easy regeneration of P-CDP.[7]

However, the non-interference hypothesis and easy regeneration of P-CDP have not been verified with a large database of MPs at environmentally relevant concentrations. To target the non-interference hypothesis, the batch kinetics and instantaneous uptake experiments will be performed in water samples from lakes and wastewater treatment plant effluents with the presence of natural water constituents. The non-interference hypothesis can be demonstrated if similar removal efficiencies for MPs are observed in experiments with complex water matrices as presented in this paper. The regeneration of P-CDP will be verified through instantaneous uptake experiments with a large mixture of over 100 MPs at environmentally relevant concentrations. The thin layer of P-CDP fixed on the filter will be saturated by passing enough volume of mixture of MPs through and then rinsed with different organic solvents such as methanol, ethanol, acetone, and acetonitrile. These processes will be repeated for several cycles until the reduced performance of P-CDP is observed. Through these regeneration experiments,

not only the regeneration property of P-CDP at environmentally relevant concentrations can be tested but also the composition of the rinse solution can be optimized.

Additionally, only two physicochemical properties of MPs have been confirmed in this research for the selectivity of P-CDP. Due to the limited number of descriptors in LSER modelling, it is very hard to achieve a goodness of fit (r^2) higher than 0.80 for the prediction model. To find out more influential properties and improve the accuracy of prediction for the affinity, a Quantitative Structure Activity Relationship (QSAR) model will be develop based on affinity experiments with a large mixture of 247 MPs. Selection of parameters out of a total number of 1875 physicochemical descriptors will be performed with the least absolute shrinkage and selection operator (Lasso) regression method. Hopefully, several more properties which impact the affinity of MPs to P-CDP (perhaps including a charge-state parameter) will be sieved out and a QSAR model with better prediction capability will be developed through the new affinity experiments and Lasso.

Together, future studies on the non-interference hypothesis, regeneration, and a comprehensive QSAR model may improve the understanding of the adsorption mechanism of P-CDP and lay the foundation for pilot-scale tests including P-CDP-UF and P-CDP packed columns.

REFERENCE

(1) Schwarzenbach, R. P.; Escher, B. I.; Fenner, K.; Hofstetter, T. B.; Johnson, C. A.; von Gunten, U.; Wehrli, B. The challenge of micropollutants in aquatic systems. *Science (80-.).* **2006**, *313* (5790), 1072–1077.

(2) Schnoor, J. L. Re-emergence of emerging contaminants. *Environ. Sci. Technol.* **2014**, *48* (19), 11019–11020.

(3) Relyea, R. A. A cocktail of contaminants: How mixtures of pesticides at low concentrations affect aquatic communities. *Oecologia* **2009**, *159* (2), 363–376.

(4) Richardson, S. D.; Ternes, T. A. Water analysis: Emerging contaminants and current issues. *Anal. Chem.* **2005**, *77* (12), 3807–3838.

(5) Helbling, D. E.; Hollender, J.; Kohler, H. P. E.; Singer, H.; Fenner, K. High-throughput identification of microbial transformation products of organic micropollutants. *Environ. Sci. Technol.* **2010**, *44* (17), 6621–6627.

(6) Rossner, A.; Snyder, S. A.; Knappe, D. R. U. Removal of emerging contaminants of concern by alternative adsorbents. *Water Res.* **2009**, *43* (15), 3787–3796.

(7) Alsbaiee, A.; Smith, B. J.; Xiao, L.; Ling, Y.; Helbling, D. E.; Dichtel, W. R. Rapid removal of organic micropollutants from water by a porous β-cyclodextrin polymer. *Nature* **2015**, *529* (7585), 190–194.

(8) Gasser, L.; Fenner, K.; Scheringer, M. Indicators for the exposure assessment of transformation products of organic micropollutants. *Environ. Sci. Technol.* **2007**, *41* (7), 2445–2451.

(9) Cui, N.; Zhang, X.; Xie, Q.; Wang, S.; Chen, J.; Huang, L.; Qiao, X.; Li, X.; Cai, X. Toxicity profile of labile preservative bronopol in water: The role of more persistent and toxic transformation products. *Environ. Pollut.* **2011**, *159* (2), 609–615.

(10) de Jesus Gaffney, V.; Almeida, C. M. M.; Rodrigues, A.; Ferreira, E.; Benoliel, M. J.; Cardoso, V. V. Occurrence of pharmaceuticals in a water supply system and related human health risk assessment. *Water Res.* **2014**, *2*, 1–10.

(11) Ternes, T. A.; Meisenheimer, M.; McDowell, D.; Sacher, F.; Brauch, H. J.; Haist-Gulde, B.; Preuss, G.; Wilme, U.; Zulei-Seibert, N. Removal of pharmaceuticals during drinking water treatment. *Environ. Sci. Technol.* **2002**, *36* (17), 3855–3863.

(12) Westerhoff, P.; Yoon, Y.; Snyder, S.; Wert, E. Fate of endocrine-disruptor, pharmaceutical, and personal care product chemicals during simulated drinking water treatment processes. *Environ. Sci. Technol.* **2005**, *39* (17), 6649–6663.

(13) Vieno, N.; Tuhkanen, T.; Kronberg, L. Removal of pharmaceuticals in drinking water treatment: effect of chemical coagulation. *Environ. Technol.* **2006**, *27* (2), 183–192.

(14) Adams, C.; Loftin, K. A.; Adams, C.; Asce, M.; Wang, Y.; Loftin, K.; Meyer, M. Removal of Antibiotics from Surface and Distilled Water in Conventional Water Treatment Processes. *J. Environ. Eng.* **2002**, *128* (MARCH), 253–260.

(15) Gibs, J.; Stackelberg, P. E.; Furlong, E. T.; Meyer, M.; Zaugg, S. D.; Lippincott, R. L. Persistence of pharmaceuticals and other organic compounds in chlorinated drinking water as a function of time. *Sci. Total Environ.* **2007**, *373* (1), 240–249.

(16) Matsui, Y.; Knappe, D. R. U.; Takagi, R. Pesticide adsorption by granular activated carbon adsorbers. 1. Effect of natural organic matter preloading on removal rates and model simplification. *Environ. Sci. Technol.* **2002**, *36* (15), 3426–3431.

(17) Matsui, Y.; Knappe, D. R. U.; Iwaki, K.; Ohira, H. Pesticide adsorption by granular activated carbon adsorbers. 2. Effects of pesticide and natural organic matter characteristics on pesticide breakthrough curves. *Environ. Sci. Technol.* **2002**, *36* (15), 3432–3438.

(18) Kennedy, A.; Summers, R. S. Effect of DOM Size on Organic Micropollutant Adsorption by GAC. *Environ. Sci. Technol.* **2015**, *49*, 6617–6624.

(19) Kennedy, A. M.; Reinert, A. M.; Knappe, D. R. U.; Ferrer, I.; Summers, R. S. Full- and pilot-scale GAC adsorption of organic micropollutants. *Water Res.* **2014**, *68C*, 238–248.

(20) Fatta-Kassinos, D.; Vasquez, M. I.; Kümmerer, K. Transformation products of pharmaceuticals in surface waters and wastewater formed during photolysis and advanced oxidation processes - Degradation, elucidation of byproducts and assessment of their biological potency. *Chemosphere* **2011**, *85* (5), 693–709.

(21) Margot, J.; Kienle, C.; Magnet, A.; Weil, M.; Rossi, L.; de Alencastro, L. F.; Abegglen, C.; Thonney, D.; Chèvre, N.; Schärer, M.; et al. Treatment of micropollutants in municipal wastewater: Ozone or powdered activated carbon? *Sci. Total Environ.* **2013**, *461-462*, 480–498.

(22) Cai, X.; Liu, Q.; Xia, C.; Shan, D.; Du, J.; Chen, J. Recyclable Capture and Destruction of Aqueous Micropollutants Using the Molecule-Specific Cavity of Cyclodextrin Polymer Coupled with KMnO 4 Oxidation. *Environ. Sci. Technol.* **2015**, *49* (15), 9264–9272.

(23) Cook, D.; Newcombe, G.; Sztajnbok, P. The application of powdered activated carbon for MIB and geosmin removal: Predicting PAC doses in four raw waters. *Water Res.* **2001**, *35* (5), 1325–1333.

(24) Oller, I.; Malato, S.; Sánchez-Pérez, J. A. Combination of Advanced Oxidation Processes and biological treatments for wastewater decontamination-A review. *Sci. Total Environ.* **2011**, *409* (20), 4141–4166.

(25) Guzzella, L.; Feretti, D.; Monarca, S. Advanced oxidation and adsorption technologies for organic micropollutant removal from lake water used as drinking-water supply. *Water Res.* **2002**, *36* (17), 4307–4318.

(26) Huber, M. M.; Canonica, S.; Park, G. Y.; Von Gunten, U. Oxidation of pharmaceuticals during ozonation and advanced oxidation processes. *Environ. Sci. Technol.* **2003**, *37* (5), 1016–1024.

(27) Shu, Z.; Bolton, J. R.; Belosevic, M.; Gamal El Din, M. Photodegradation of emerging micropollutants using the medium-pressure UV/H2O2 Advanced Oxidation Process. *Water Res.* **2013**, *47* (8), 2881–2889.

(28) Ling, Y.; Long, M.; Hu, P.; Chen, Y.; Huang, J. Magnetically separable core-shell structural γ-Fe2O3@Cu/Al-MCM-41 nanocomposite and its performance in heterogeneous Fenton catalysis. *J. Hazard. Mater.* **2014**, *264*, 195–202.

(29) Schröder, H. F.; Meesters, R. J. W. Stability of fluorinated surfactants in advanced oxidation processes - A follow up of degradation products using flow injection-mass spectrometry, liquid chromatography-mass spectrometry and liquid chromatography-multiple stage mass spectrometry. *J. Chromatogr. A* **2005**, *1082* (1 SPEC. ISS.), 110–119.

(30) Rosal, R.; Gonzalo, M. S.; Boltes, K.; Leton, P.; Vaquero, J. J.; Garcia-Calvo, E. Identification of intermediates and assessment of ecotoxicity in the oxidation products generated during the ozonation of clofibric acid. *J. Hazard. Mater.* **2009**, *172* (2-3), 1061–1068.

(31) Sirtori, C.; Aguera, A.; Gernjak, W.; Malato, S. Effect of water-matrix composition on Trimethoprim solar photodegradation kinetics and pathways. *Water Res.* **2010**, *44* (9), 2735–2744.

(32) Benner, J.; Helbling, D. E.; Kohler, H.-P. E.; Wittebol, J.; Kaiser, E.; Prasse, C.; Ternes, T. A.; Albers, C. N.; Aamand, J.; Horemans, B.; et al. Is biological treatment a viable alternative for micropollutant removal in drinking water treatment processes? *Water Res.* **2013**, *47* (16), 5955–5976.

(33) Munoz, I.; Rieradevall, J.; Torrades, F.; Peral, J.; Domenech, X. Environmental assessment of different solar driven advanced oxidation processes. *Sol. Energy* **2005**, *79* (4), 369–375.

(34) Radjenovic, J.; Petrovic, M.; Ventura, F.; Barcelo, D. Rejection of pharmaceuticals in nanofiltration and reverse osmosis membrane drinking water treatment. *Water Res.* **2008**, *42* (14), 3601–3610.

(35) Al-Rifai, J. H.; Khabbaz, H.; Schafer, A. I. Removal of pharmaceuticals and endocrine disrupting compounds in a water recycling process using reverse osmosis systems. *Sep. Purif. Technol.* **2011**, *77* (1), 60–67.

(36) Potts, D. E.; Ahlert, R. C.; Wang, S. S. A critical review of fouling of reverse osmosis membranes. *Desalination* **1981**, *36*, 235–264.

(37) Vrijenhoek, E. M.; Hong, S.; Elimelech, M. Influence of membrane surface properties on initial rate of colloidal fouling of reverse osmosis and nanofiltration membranes. *J. Memb. Sci.* **2001**, *188* (1), 115–128.

(38) Kumar, M.; Adham, S. S.; Pearce, W. R. Investigation of seawater reverse osmosis fouling and its relationship to pretreatment type. *Environ. Sci. Technol.* **2006**, *40* (6), 2037–2044.

(39) Knappe, D. R. U.; Snoeyink, V. L.; Roche, P.; Prados, M. J.; Bourbigot, M. M. Atrazine removal by preloaded GAG. *Am. Water Work. Assoc.* **1999**, *91* (10), 97–109.

(40) Rossner, A.; Knappe, D. R. U. MTBE adsorption on alternative adsorbents and packed bed adsorber performance. *Water Res.* **2008**, *42* (8-9), 2287–2299.

(41) Li, L.; Quinlivan, P. A.; Knappe, D. R. U. Predicting adsorption isotherms for aqueous organic micropollutants from activated carbon and pollutant properties. *Environ. Sci. Technol.* **2005**, *39* (9), 3393–3400.

(42) San Miguel, G.; Lambert, S. D.; Graham, N. J. D. The regeneration of field-spent granular-activated carbons. *Water Res.* **2001**, *35* (11), 2740–2748.

(43) Gagné, F.; Bouchard, B.; André, C.; Farcy, E.; Fournier, M. Evidence of feminization in wild Elliptio complanata mussels in the receiving waters downstream of a municipal effluent outfall. *Comp. Biochem. Physiol. - C Toxicol. Pharmacol.* **2011**, *153* (1), 99–106.

(44) Tetreault, G. R.; Bennett, C. J.; Shires, K.; Knight, B.; Servos, M. R.; McMaster, M. E. Intersex and reproductive impairment of wild fish exposed to multiple municipal wastewater discharges. *Aquat. Toxicol.* **2011**, *104* (3-4), 278–290.

(45) Pomati, F.; Castiglioni, S.; Zuccato, E.; Fanelli, R.; Vigetti, D.; Rossetti, C.; Calamari, D. Effects of a Complex Mixture of Therapeutic Drugs at Environmental Levels on Human Embryonic Cells. *Environ. Sci. Technol.* **2006**, *40* (7), 2442–2447.

(46) Bonvin, F.; Jost, L.; Randin, L.; Bonvin, E.; Kohn, T. Super-fine powdered activated carbon (SPAC) for efficient removal of micropollutants from wastewater treatment plant effluent. *Water Res.* **2015**, *90*, 90–99.

(47) Boehler, M.; Zwickenpflug, B.; Hollender, J.; Ternes, T.; Joss, A.; Siegrist, H. Removal of micropollutants in municipal wastewater treatment plants by powder-activated carbon. *Water Sci. Technol.* **2012**, *66* (10), 2115–2121.

(48) Kovalova, L.; Knappe, D. R. U.; Lehnberg, K.; Kazner, C.; Hollender, J. Removal of highly polar micropollutants from wastewater by powdered activated carbon. *Environ. Sci. Pollut. Res.* **2013**, *20* (6), 3607–3615.

(49) Li, X.; Zhao, H.; Quan, X.; Chen, S.; Zhang, Y.; Yu, H. Adsorption of ionizable organic contaminants on multi-walled carbon nanotubes with different oxygen contents. *J. Hazard. Mater.* **2011**, *186* (1), 407–415.

(50) Nam, S.-W.; Choi, D.-J.; Kim, S.-K.; Her, N.; Zoh, K.-D. Adsorption characteristics of selected hydrophilic and hydrophobic micropollutants in water using activated carbon. *J. Hazard. Mater.* **2014**, *270*, 144–152.

(51) Ali, I.; Asim, M.; Khan, T. A. Low cost adsorbents for the removal of organic pollutants from wastewater. *J. Environ. Manage.* **2012**, *113*, 170–183.

(52) Connors, K. A. The Stability of Cyclodextrin Complexes in Solution. *Chem. Rev.* **1997**, *97* (5), 1325–1357.

(53) Liu, H.; Cai, X.; Wang, Y.; Chen, J. Adsorption mechanism-based screening of cyclodextrin polymers for adsorption and separation of pesticides from water. *Water Res.* **2011**, *45* (11), 3499–3511.

(54) Morin-Crini, N.; Crini, G. Environmental applications of water-insoluble β-cyclodextrin-epichlorohydrin polymers. *Prog. Polym. Sci.* **2013**, *38* (2), 344–368.

(55) Szejtli, J. Introduction and General Overview of Cyclodextrin Chemistry. *Chem. Rev.* **1998**, *98* (97), 1743–1753.

(56) Zoschke, K.; Engel, C.; Börnick, H.; Worch, E. Adsorption of geosmin and 2-methylisoborneol onto powdered activated carbon at non-equilibrium conditions: Influence of NOM and process modelling. *Water Res.* **2011**, *45* (15), 4544–4550.

(57) Helbling, D. E.; Johnson, D. R.; Honti, M.; Fenner, K. Micropollutant Biotransformation Kinetics Associate with WWTP Process Parameters and Microbial Community Characteristics. *Environ. Sci. Technol.* **2012**, *46* (19), 10579–10588.

(58) Liu, H.; Cai, X.; Chen, J. Mathematical model for cyclodextrin alteration of bioavailability of organic pollutants. *Environ. Sci. Technol.* **2013**, *47* (11), 5835–5842.

(59) Ho, Y. S.; McKay, G. Pseudo-second order model for sorption processes. *Process Biochem.* **1999**, *34* (5), 451–465.

(60) Kamlet, M. J.; Doherty, R. M.; Abraham, M. H.; Taft, R. W. Linear solvation energy relationships. 33. An analysis of the factors that influence adsorption of organic compounds on activated carbon. *Carbon N. Y.* **1985**, *23* (5), 549–554.

(61) Yap, C. W. PaDEL-descriptor: an open source software to calculate molecular descriptors and fingerprints. *J. Comput. Chem.* **2011**, *32* (7), 1466–1474.

(62) Platts, J. A.; Butina, D.; Abraham, M. H.; Hersey, A. Estimation of molecular linear free energy relation descriptors using a group contribution approach. *J. Chem. Inf. Model.* **1999**, *39* (5), 835–845.

(63) Huntscha, S.; Singer, H. P.; McArdell, C. S.; Frank, C. E.; Hollender, J. Multiresidue analysis of 88 polar organic micropollutants in ground, surface and wastewater using online mixed-bed multilayer solid-phase extraction coupled to high performance liquid chromatography-tandem mass spectrometry. *J. Chromatogr. A* **2012**, *1268*, 74–83.

(64) Li, L.; Quinlivan, P. A.; Knappe, D. R. U. Effects of activated carbon surface chemistry and pore structure on the adsorption of organic contaminants from aqueous solution. *Carbon N. Y.* **2002**, *40* (12), 2085–2100.

(65) Bausk, A. S.; Dvorak, B. I. Selecting the column configuration with lowest media replacement cost for small adsorption systems. *Water Res.* **2016**, *93*, 38–47.

(66) Alhamed, Y. A. Adsorption kinetics and performance of packed bed adsorber for phenol removal using activated carbon from dates' stones. *J. Hazard. Mater.* **2009**, *170* (2-3), 763–770.

(67) Xia, X.-R.; Monteiro-Riviere, N. A.; Riviere, J. E. An index for characterization of nanomaterials in biological systems. *Nat. Nanotechnol.* **2010**, *5* (9), 671–675.

(68) Apul, O. G.; Wang, Q.; Shao, T.; Rieck, J. R.; Karanfil, T. Predictive model development for adsorption of aromatic contaminants by multi-walled carbon nanotubes. *Environ. Sci. Technol.* **2013**, *47* (5), 2295–2303.

(69) Chen, L.; Dionysiou, D. D.; O'Shea, K. Complexation of microcystins and nodularin by cyclodextrins in aqueous solution, a potential removal strategy. *Environ. Sci. Technol.* **2011**, *45* (6), 2293–2300.

(70) Matsui, Y.; Yoshida, T.; Nakao, S.; Knappe, D. R. U.; Matsushita, T. Characteristics of competitive adsorption between 2-methylisoborneol and natural organic matter on

superfine and conventionally sized powdered activated carbons. *Water Res.* **2012**, *46* (15), 4741–4749.

(71) Quinlivan, P. A.; Li, L.; Knappe, D. R. U. Effects of activated carbon characteristics on the simultaneous adsorption of aqueous organic micropollutants and natural organic matter. *Water Res.* **2005**, *39* (8), 1663–1673.

(72) Kilduff, J. E.; Karanfil, T.; Weber, W. J. J. Competitive Effects of Nondisplaceable Organic Compounds on Trichloroethylene Uptake by Activated Carbon. II. Model Verification and Applicability to Natural Organic Matter. *J. Colloid Interface Sci.* **1998**, *205* (2), 280–289.

(73) Kilduff, J. E.; Karanfil, T.; Weber, W. J. J. Competitive Effects of Nondisplaceable Organic Compounds on Trichloroethylene Uptake by Activated Carbon. I. Thermodynamic Predictions and Model Sensitivity Analyses. *J. Colloid Interface Sci.* **1998**, *205* (2), 271–279.

(74) Carter, M. C.; Weber, W. J.; Olmestead, K. P. Effects of background dissolved organic matter on TCE adsorption by GAC. *Am. Water Work. Assoc.* **1992**, *84* (8), 81–91.

(75) Mamba, B. B.; Krause, R. W.; Malefetse, T. J.; Sithole, S. P.; Nkambule, T. I. Humic acid as a model for natural organic matter (NOM) in the removal of odorants from water by cyclodextrin polyurethanes. *Water SA* **2009**, *35* (1), 117–120.

APPENDIX

A. Information of 90 representative MPs

Table A1: Characteristics of all ninety micropollutants.

No.[a]	Compound Name	CAS #	Supplier	Chemical Formula	pKa[b]	$logK_{ow}$[c]	Charge[d]
1	2,4-D	94-75-7	Aldrich	C8H6Cl2O3	3.0±0.1	2.50	-
2	Abacavir	136470-78-5	Aldrich	C14H18N6O	14.9±0.1	0.39	n
3	Acebutolol	37517-30-9	Aldrich	C18H28N2O4	13.8±0.2	1.53	+
4	Acetaminophen	103-90-2	USP	C8H9NO2	9.9±0.1	0.91	n
5	Acetochlor	34256-82-1	Aldrich	C14H20ClNO2	1.3±0.5	3.50	n
6	Albuterol	18559-94-9	Aldrich	C13H21NO3	10.0±0.3	0.34	+
7	Allopurinol	315-30-0	Aldrich	C5H4N4O	9.2±0.5	0.35	n
8	Amphetamine	300-62-9	Aldrich	C9H13N	9.9±0.1	1.80	+
9	Atenolol	29122-68-7	Aldrich	C14H22N2O3	13.9±0.2	0.43	+
10	Atenolol Acid	56392-14-4	Aldrich	C14H21N1O4	4.4±0.1	-1.24	z
11	Atrazine	1912-24-9	Aldrich	C8H14Cl1N5	2.3±0.1	1.76	n
12	Benzotriazole-methyl-1H	136-85-6	Aldrich	C7H7N3	8.7±0.4	1.81	n
13	Bromacil	314-40-9	Aldrich	C9H13BrN2O2	8.8±0.4	1.69	z
14	Bupropion	34841-39-9	Cerilliant	C13H18ClNO	N/A	3.27	+
15	Caffeine	58-08-2	USP	C8H10N4O2	0.5±0.7	-0.55	n
16	Carbamazepine	298-46-4	Aldrich	C15H12N2O	13.9±0.2	2.77	n
17	Carbaryl	63-25-2	Aldrich	C12H11NO2	12.0±0.5	2.96	n
18	Carbofuran	1563-66-2	Aldrich	C12H15NO3	12.3±0.5	1.30	n
19	Chloridazon	1698-60-8	Aldrich	C10H8Cl1N3O1	0.7±0.2	1.11	n
20	Chloroxylenol	88-04-0	Aldrich	C8H9ClO	9.8±0.2	3.30	n
21	Cimetidine	51481-61-9	Aldrich	C10H16N6S	14.1±0.1	-0.29	n
22	Clofibric Acid	882-09-7	Aldrich	C10H11ClO3	3.2±0.1	2.90	-
23	Codeine	76-57-3	Cerilliant	C18H21NO3	13.4±0.2	1.34	+
24	Cotinine	486-56-6	Cerilliant	C10H12N2O	4.7±0.1	0.21	n
25	DEET	134-62-3	Aldrich	C12H17NO	-1.4±0.7	2.50	n
26	Diazinon	333-41-5	Aldrich	C12H21N2O3P1S1	1.2±0.3	4.19	n
27	Diclofenac	15307-86-5	Aldrich	C14H11Cl2N1O2	4.2±0.1	4.60	-
28	Dimethoate	60-51-5	Aldrich	C5H12NO3PS2	14.4±0.5	-1.48	n
29	Diuron	330-54-1	Aldrich	C9H10Cl2N2O1	13.6±0.7	2.30	n
30	Efavirenz	154598-52-4	Aldrich	C14H9ClF3NO2	10.2±0.4	5.15	n

31	Erythromycin	114-07-8	Aldrich	C37H67NO13	13.1±0.7	2.60	+
32	Estrone	53-16-7	Aldrich	C18H22O2	10.3±0.4	4.31	n
33	Famotidine	76824-35-6	Aldrich	C8H15N7O2S3	7.5±0.4	-1.95	+
34	Fluconazole	86386-73-4	Aldrich	C13H12F2N6O	11.0±0.3	0.56	n
35	Fluoxetine	54910-89-3	Aldrich	C17H18F3NO	10.1±0.1	4.17	+
36	Gemfibrozil	25812-30-0	Aldrich	C15H22O3	4.8± 0.5	4.39	-
37	Hydrocodone	125-29-1	Cerilliant	C18H21NO3	8.5±0.2	1.96	+
38	Ibuprofen	15687-27-1	Arcos Organics	C13H18O2	4.4±0.1	3.84	-
39	Imidacloprid	138261-41-3	Aldrich	C9H10ClN5O2	7.2±0.2	-0.59	z
40	Iopromid	73334-07-3	Aldrich	C18H24I3N3O8	10.6±0.7	-0.44	z
41	Ioxynil	1689-83-4	Aldrich	C7H3I2NO	5.0±0.2	3.38	-
42	Isoproturon	34123-59-6	Aldrich	C12H18N2O1	15.1±0.7	2.57	n
43	Ketoprofen	22071-15-4	Aldrich	C16H14O3	4.2±0.1	3.61	-
44	Linuron	330-55-2	Aldrich	C9H10Cl2N2O2	12.1±0.7	2.30	n
45	Malaoxon	1634-78-2	Aldrich	C10H19O7PS	N.A	0.97	n
46	MCPA	94-74-6	Aldrich	C9H9ClO3	3.1±0.1	2.41	-
47	Mecoprop	93-65-2	Aldrich	C10H11ClO3	3.2±0.1	2.98	-
48	Meprobamate	57-53-4	Cerilliant	C9H18N2O4	13.1±0.5	0.93	n
49	Methomyl	16752-77-5	Aldrich	C5H10N2O2S	13.3±0.5	0.72	n
50	Metolachlor	51218-45-2	Aldrich	C15H22ClNO2	1.5±0.5	3.45	n
51	Metoprolol	37350-58-6	Aldrich	C15H25NO3	13.9±0.2	1.76	+
52	Metribuzin	21087-64-9	Aldrich	C8H14N4O1S1	-0.2±0.2	1.96	n
53	Molinate	2212-67-1	Aldrich	C9H17NOS	-1.2±0.2	2.34	n
54	Morphine	57-27-2	Cerilliant	C17H19O3	9.5±0.4	0.90	+
55	Nadolol	42200-33-9	Aldrich	C17H27NO4	13.9±0.2	0.87	+
56	Naproxen	22204-53-1	Aldrich	C14H14O3	4.8±0.3	2.99	-
57	Oxcarbazepine	28721-07-5	Aldrich	C15H12N2O2	13.7±0.2	1.82	n
58	Oxybenzone	131-57-7	Aldrich	C14H12O3	7.6±0.4	3.62	-
59	Paraxanthine	611-59-6	Aldrich	C7H8N4O2	8.5±0.5	0.09	n
60	Penciclovir	39809-25-1	Aldrich	C10H15N5O3	14.4±0.1	-1.69	n
61	Pentoxyfylline	6493-05-6	Aldrich	C13H18N4O3	0.5±0.7	0.23	n
62	PFBA	375-22-4	Aldrich	C4HF7O2	0.4±0.1	2.31	-
63	PFOA	335-67-1	Aldrich	C8HF15O2	0.5±0.1	5.11	-
64	Phenytoin	57-41-0	Aldrich	C15H12N2O2	8.3±0.1	3.40	z
65	Progesterone	57-83-0	Aldrich	C21H30O2	N.A	4.15	n
66	Prometon	1610-18-0	Aldrich	C10H19N5O	4.4±0.41	1.75	n

67	Propachlor	1918-16-7	Aldrich	C11H14ClNO	0.3±0.5	2.39	n
68	Ranitidine	66357-35-5	USP	C13H22N4O3S	8.4±0.3	0.99	z
69	Siduron	1982-49-6	Aldrich	C14H20N2O	12.4±0.4	3.27	n
70	Simazine	122-34-9	Aldrich	C7H12ClN5	2.7±0.1	0.63	n
71	Sitagliptin	486460-32-6	Aldrich	C16H15F6N5O	7.2±0.1	1.26	+
72	Sucralose	56038-13-2	Aldrich	C12H19Cl3O8	12.5±0.7	-0.47	n
73	Sulfamethoxazole	723-46-6	Aldrich	C10H11N3O3S	5.8±0.5	0.79	-
74	Sulfathiazole	72-14-0	Aldrich	C9H9N3O2S2	7.2±0.1	0.98	-
75	TCEP	115-96-8	Aldrich	C6H12Cl3O4P	N.A	2.11	n
76	Testosterone	58-22-0	Aldrich	C19H28O2	15.1±0.6	3.37	n
77	Tramadol	27203-92-5	Cerilliant	C16H25NO2	14.5±0.4	2.45	+
78	Tributyl Phosphate	126-73-8	Aldrich	C12H27O4P	N.A	4.09	n
79	Triclosan	3380-34-5	Aldrich	C12H7Cl3O2	7.8±0.4	4.98	n
80	Trimethoprim	738-70-5	Aldrich	C14H18N4O3	7.0±0.1	0.89	+
81	Valsartan	137862-53-4	USP	C24H29N5O3	3.6±0.1	5.27	-
82	Venlafaxine	93413-69-5	USP	C17H27NO2	14.8±0.2	2.74	+
83	Warfarin	81-81-2	Aldrich	C19H16O4	4.5±1.0	3.52	-
84[e]	Aldicarb	116-06-3	Aldrich	C7H14O2N2S1	13.8±0.5	1.28	n
85[e]	Bentazon	25057-89-0	Aldrich	C10H12N2O3S	3.3±0.7	0.76	-
86[e]	Beta-Estradiol	50-28-2	Aldrich	C18H24O2	10.3±0.6	3.75	n
87[e]	Dextromethorphan	125-71-3	Aldrich	C18H25NO	9.1±0.2	3.49	+
88[e]	Estriol	50-27-1	Aldrich	C18H24O3	10.3±0.7	2.67	n
89[e]	Ethynylestradiol	57-63-6	Aldrich	C20H24O2	10.2±0.6	3.90	n
90[e]	Glyphosate	1071-83-6	Aldrich	C3H8NO5P	1.2±0.1	-3.10	z

a. Number is used to tag the respective MP for future reference;
b. pK_a was found on Scifinder. N.A. means that no pK_a was reported for that MP;
c. $\log K_{ow}$ are estimated values obtained from Marvin from ChemAxon;
d. Charge state was predicted by Marvin from ChemAxon at pH = 7.4.
e. MPs from No.84 (Aldicarb) to No.90 (Glyphosate) are not amenable to analysis by analytical methods adopted in this research.

Table A2: Analytical data required for the 83 MPs amenable to the analytical method.

No.	Compound Name	Exact Mass [M]	Ionization Mode[a]	Retention Time[b]	LOQ[c]
1	2,4-D	219.9689	negative	14.03	10
2	Abacavir	286.1542	positive	9.25	1
3	Acebutolol	336.2049	positive	10.11	1
4	Acetaminophen	151.0628	positive	8.32	10
5	Acetochlor	269.1177	positive	16.20	10
6	Albuterol	239.1521	positive	8.12	1
7	Allopurinol	136.0385	positive	7.35	200
8	Amphetamine	135.1048	positive	9.30	1
9	Atenolol	266.1625	positive	8.16	1
10	Atenolol Acid	267.1471	positive	9.24	1
11	Atrazine	215.0932	positive	13.17	1
12	Benzotriazole-methyl-1H	133.0635	positive	11.12	1
13	Bromacil	260.0155	positive	12.03	10
14	Bupropion	239.1077	positive	10.92	1
15	Caffeine	194.0798	positive	9.44	1
16	Carbamazepine	236.0944	positive	12.55	1
17	Carbaryl	201.0795	positive	12.52	10
18	Carbofuran	221.1057	positive	12.02	1
19	Chloridazon	221.0350	positive	10.62	1
20	Chloroxylenol	156.0342	negative	15.26	200
21	Cimetidine	252.1157	positive	8.31	1
22	Clofibric Acid	214.0391	negative	14.70	10
23	Codeine	299.1521	positive	8.52	10
24	Cotinine	176.0950	positive	6.93	50
25	DEET	191.1305	positive	13.31	1
26	Diazinon	304.1005	positive	17.47	1
27	Diclofenac	295.0161	positive	17.36	10
28	Dimethoate	229.0002	positive	10.52	1
29	Diuron	232.0165	positive	13.88	10
30	Efavirenz	315.0274	positive	17.39	10
31	Erythromycin	733.4607	positive	13.20	200
32	Estrone	270.1620	positive	11.72	1
33	Famotidine	337.0449	positive	8.29	10
34	Fluconazole	306.1035	positive	10.43	50

35	Fluoxetine	309.1335	positive	14.06	10
36	Gemfibrozil	250.1563	positive	19.30	10
37	Hydrocodone	299.1521	positive	8.82	1
38	Ibuprofen	206.1301	positive	17.76	10
39	Imidacloprid	255.0523	positive	10.06	1
40	Iopromid	790.8692	positive	8.43	1
41	Ioxynil	370.8299	negative	14.26	1
42	Isoproturon	206.1414	positive	13.56	1
43	Ketoprofen	254.0937	positive	14.30	10
44	Linuron	248.0114	positive	14.87	10
45	Malaoxon	314.0589	positive	12.06	1
46	MCPA	200.0235	negative	14.37	1
47	Mecoprop	214.0391	negative	15.60	1
48	Meprobamate	218.1267	positive	11.28	10
49	Methomyl	162.0463	positive	9.20	1
50	Metolachlor	283.1334	positive	16.35	1
51	Metoprolol	267.1829	positive	10.23	1
52	Metribuzin	214.0883	positive	11.99	1
53	Molinate	187.1031	positive	15.37	1
54	Morphine	285.1359	positive	7.52	10
55	Nadolol	309.1935	positive	9.40	1
56	Naproxen	230.0937	positive	14.83	1
57	Oxcarbazepine	252.0899	positive	11.61	10
58	Oxybenzone	228.0781	positive	16.72	50
59	Paraxanthine	180.0647	positive	8.78	10
60	Penciclovir	253.1175	positive	8.34	1
61	Pentoxyfylline	278.1379	positive	10.54	1
62	PFBA	213.9870	negative	10.70	10
63	PFOA	413.9743	negative	16.99	1
64	Phenytoin	252.0899	positive	12.36	1
65	Progesterone	314.2246	positive	17.29	10
66	Prometon	225.1584	positive	11.62	1
67	Propachlor	211.0758	positive	13.39	1
68	Ranitidine	314.1407	positive	8.24	10
69	Siduron	232.1576	positive	14.84	10
70	Simazine	201.0776	positive	11.92	1
71	Sitagliptin	407.1181	positive	10.42	10

72	Sucralose	396.0146	negative	9.90	1
73	Sulfamethoxazole	253.0516	positive	10.00	10
74	Sulfathiazole	255.0131	positive	8.58	10
75	TCEP	283.9539	positive	12.19	1
76	Testosterone	288.2089	positive	15.40	1
77	Tramadol	263.1885	positive	10.11	1
78	Tributyl Phosphate	266.1647	positive	18.87	1
79	Triclosan	287.9506	negative	19.36	10
80	Trimethoprim	290.1373	positive	9.21	1
81	Valsartan	435.2270	positive	15.60	10
82	Venlafaxine	277.2036	positive	11.28	10
83	Warfarin	308.1043	positive	15.27	1

a. The major ionization mode of the respective MP after electrospray ionization (ESI);
b. The retention time of the respective MP (in minutes);
c. The limit of quantification of the respective MP (in ng L^{-1});

B. Characterization of P-CDP and CCAC

a. Surface area and pore size distribution[a]

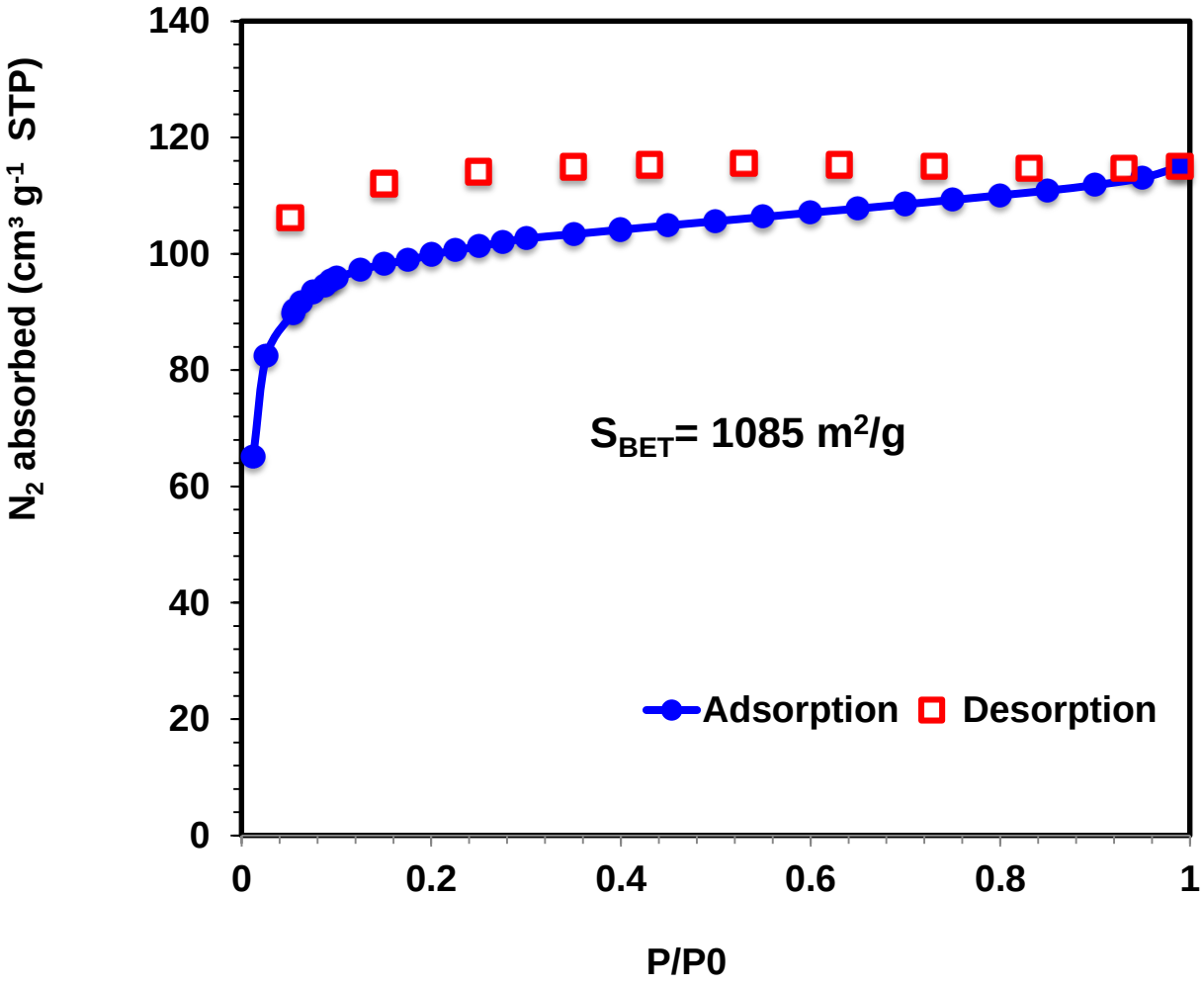

Figure B1: N_2 adsorption (blue squares) and desorption (red squares) isotherms of CCAC. The solid line is a guide to the eye.

S_{BET} is the Brunauer-Emmett-Teller (BET) surface area ($m^2\ g^{-1}$) of CCAC calculated from the N_2 adsorption isotherm, and P and P_0 are the equilibrium and saturation pressures of N_2 at 77 K, respectively.

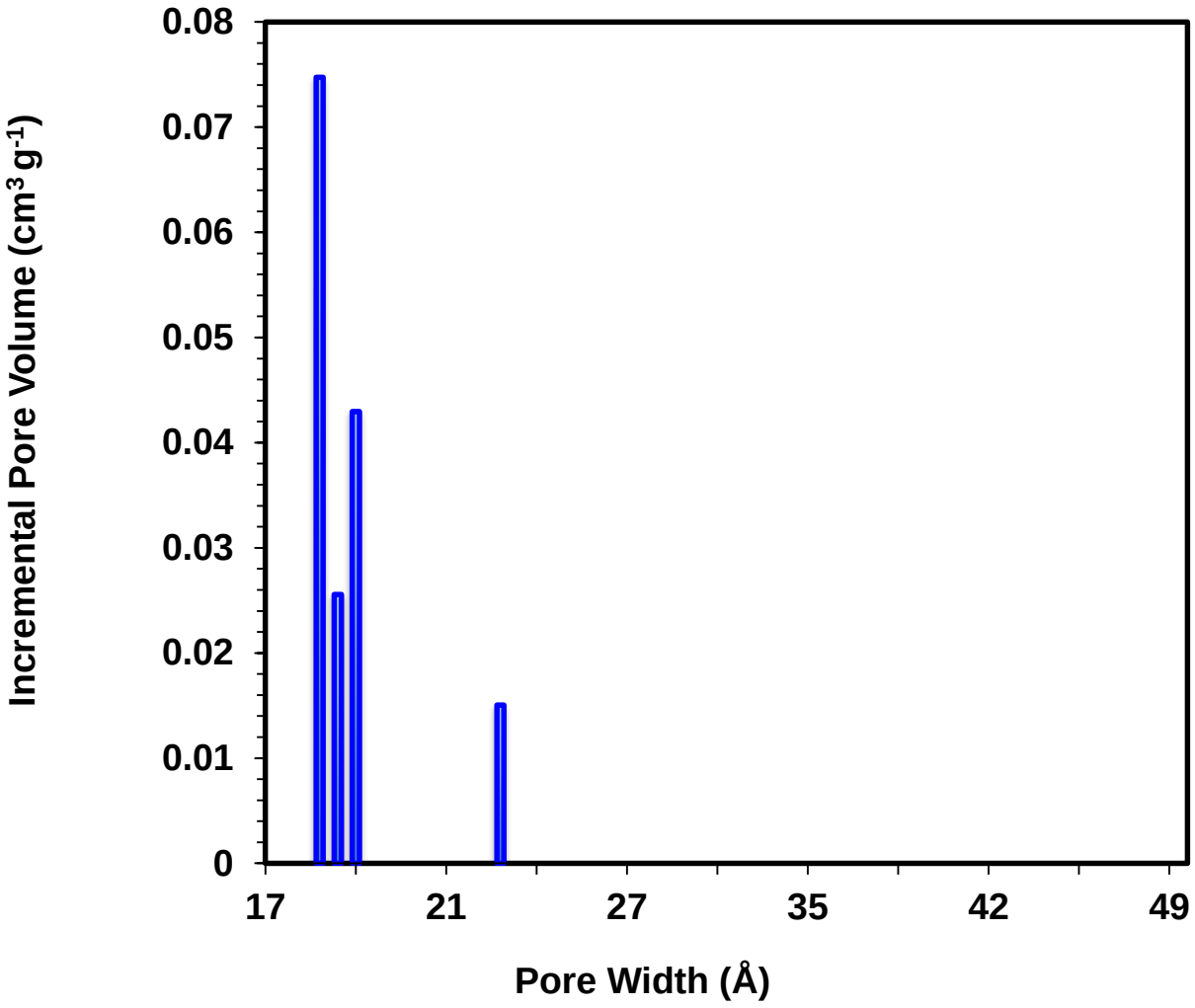

Figure B2: The incremental pore volume of CCAC obtained by Non-Local Density Functional Theory analysis.

NLDFT calculations applied to the N_2 adsorption isotherms indicate a high pore volume distributed over the range of pore width from 15 to 25 Å suggesting a mesoporous structure of CCAC.

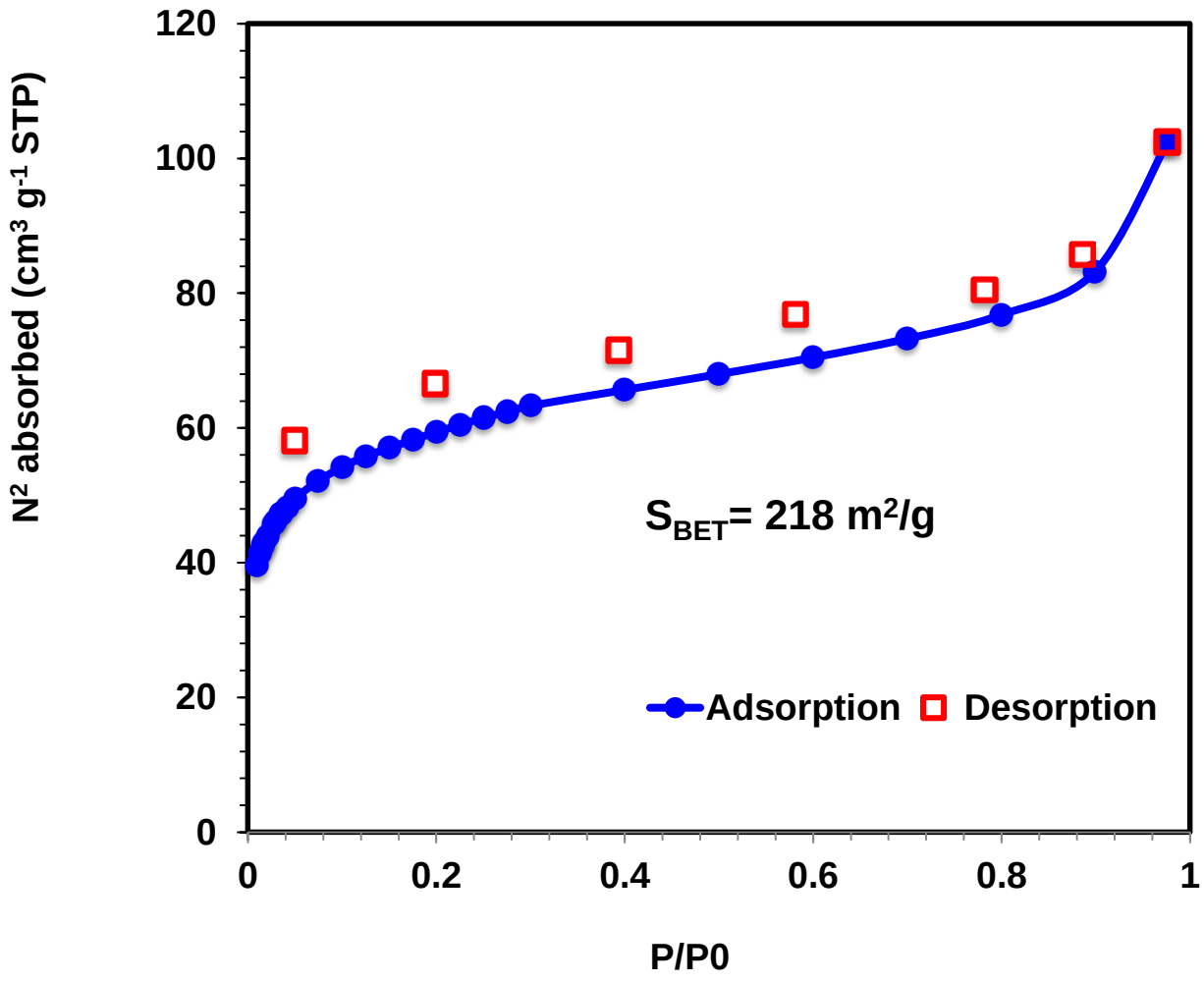

Figure B3: N_2 adsorption (blue squares) and desorption (grey squares) isotherms of P-CDP. The solid line is a guide to the eye.

S_{BET} is the Brunauer–Emmett–Teller surface area (of m^2 g^{-1}) of P-CDP calculated from the N_2 adsorption isotherm, and P and P_0 are the equilibrium and saturation pressures of N_2 at 77 K, respectively. N_2 porosimetry of the P-CDPs provided type II isotherms indicative of mesoporosity.

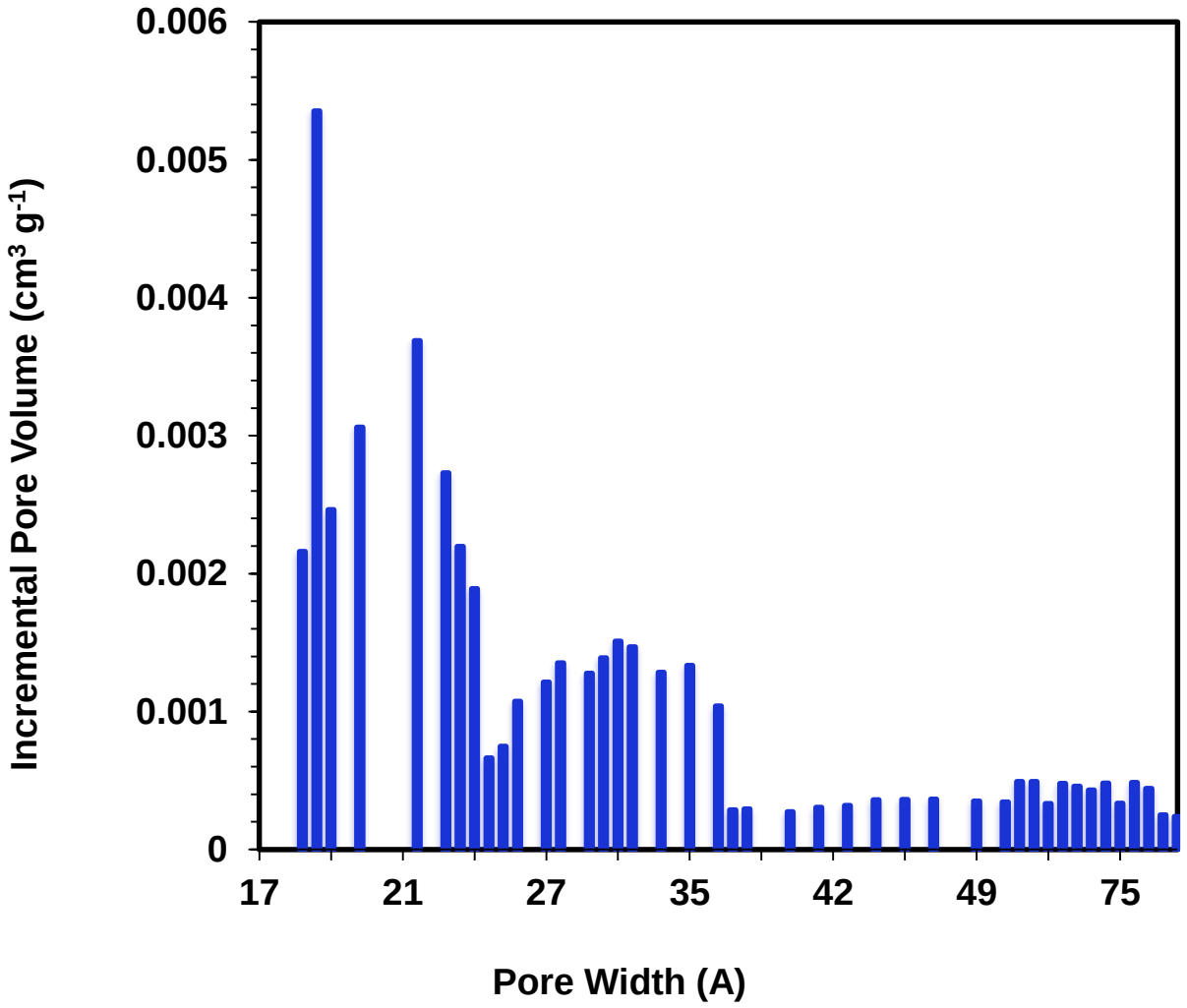

Figure B4: The incremental pore volume of P-CDP obtained by Non-Local Density Functional Theory analysis.

NLDFT calculations applied to the N_2 adsorption isotherms present the pore volume distributed over a broad range of pore width from 15 to 80 Å indicating the less-order mesoporous structure of P-CDP as compared with CCAC.

b. FT-IR spectra[b]

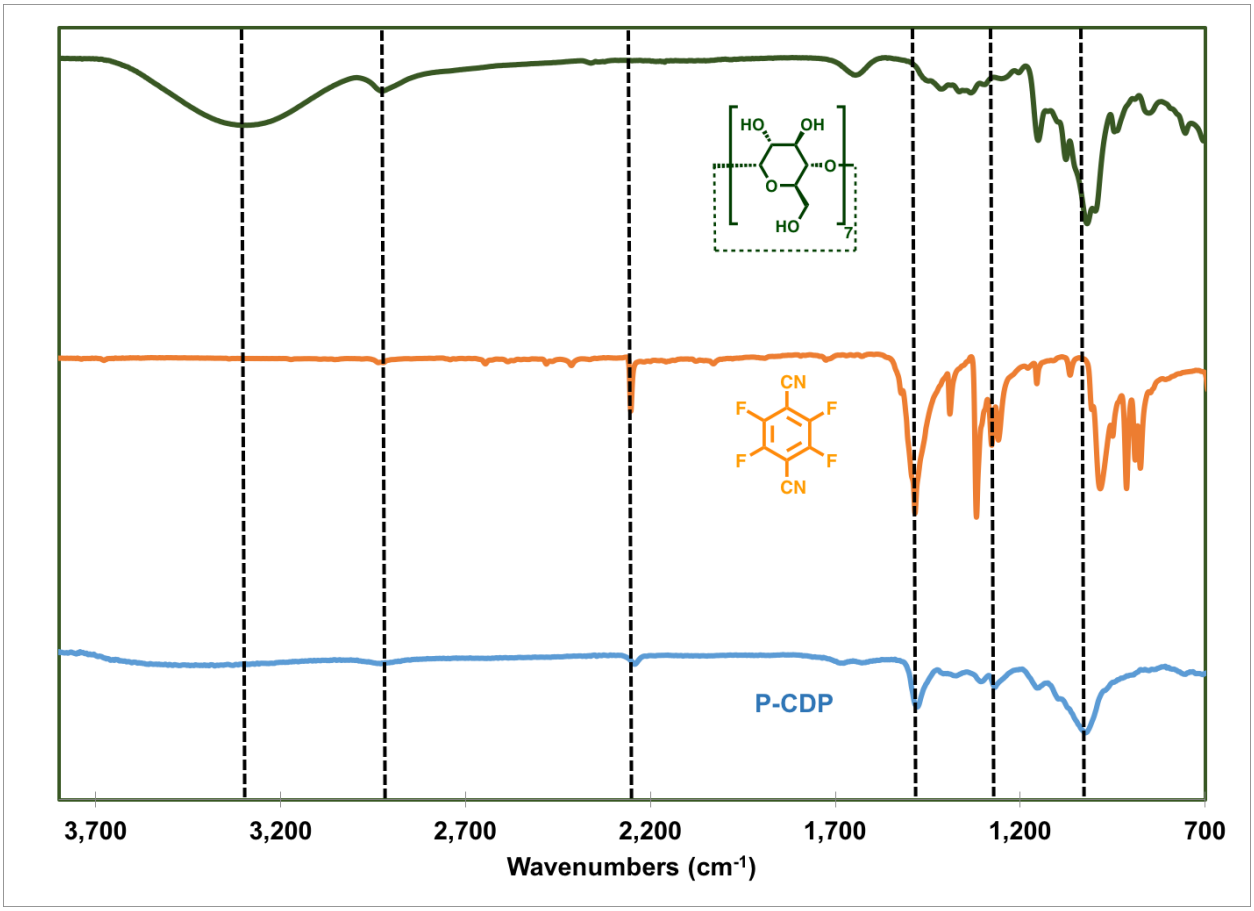

Figure B5: FT-IR spectra, Spectra are labelled by chemical structure or compound name (top trace marked as green is β-cyclodextrin, second trace marked as orange down is tetrafluoroterephthalonitrile). The FT-IR spectra shown in this figure of P-CDP reflect the incorporation of β-CD and tetrafluoroterephthalonitrile.

FTIR spectra of P-CDP showed absorbance at 2,242 cm^{-1}, corresponding to the nitrile valence vibrations. Absorption at 1,678 cm^{-1}, 1,628 cm^{-1} and 1,479 cm^{-1} can be assigned to C–C aromatic stretches. C–F stretches, which resonate at 1,307 cm^{-1} and 1,269 cm^{-1}, are present in the spectra of P-CDP and appear weaker compared to the region around 1,300 cm^{-1} in the spectrum of tetrafluoroterephthalonitrile, as expected for partial F substitution. Finally, the IR spectra of P-CDP exhibited valence vibrations of O-H bonds in the hydroxyl groups of β-CD near 3,378cm^{-1}, aliphatic C–H stretches around 2,929 cm^{-1}, and an intense C–O stretch at 1,024 cm^{-1}, which are spectral features of intact β-CD.

a. Surface area measurements were conducted on a Micromeritics ASAP 2020 Accelerated Surface Area and Porosimetry Analyzer. Each sample (25-50 mg) was degassed at 90 °C for 24 h and then backfilled with N_2. N_2 adsorption isotherms were generated by incremental exposure to ultrahigh-purity nitrogen up to 1 atm in a liquid nitrogen (77 K) bath, and surface parameters were determined using BET adsorption models included in the instrument software (Micromeritics ASAP 2020 V4.00);
b. FT-IR was performed on a Thermo Nicolet iS10 with a diamond ATR attachment.

C. Data of LSER model

Table C1: Experimental and predicted values of the distribution coefficient $log\ K_{\infty}$, solvatochromatic descriptors, and group information of all sixty compounds used in LSER model training and verification.

Compound Name	$logK_{\infty}$ [a]	$logK_{\infty}$ [b]	α^H	β^H	π^H	R	V^c	Group
2,4-D	0.45	0.73	0.50	0.60	1.24	1.09	1.38	Validation
Abacavir	3.12	2.74	0.76	2.85	2.29	1.78	2.09	Training
Acetaminophen	0.72	0.48	0.89	0.89	1.32	1.20	1.17	Training
Acetochlor	2.45	2.28	0.00	0.70	1.71	1.20	2.14	Training
Albuterol	2.21	2.36	1.08	1.90	1.45	1.31	1.98	Validation
Allopurinol	-0.49	-0.09	0.74	1.07	1.58	1.46	0.88	Training
Atenolol	2.79	2.59	0.45	1.72	1.54	1.48	2.18	Training
Atenolol Acid	3.00	2.48	0.69	1.54	1.37	1.13	2.14	Validation
Atrazine	1.63	1.39	0.65	2.18	1.51	1.22	1.62	Training
Bromacil	1.07	1.37	0.35	1.75	1.75	1.36	1.63	Validation
Caffeine	0.68	0.56	0.00	1.31	1.00	1.60	1.36	Training
Carbamazepine	1.50	1.85	0.46	0.63	1.45	1.76	1.81	Training
Carbaryl	1.38	1.25	0.35	0.91	1.55	1.77	1.54	Validation
Carbofuran	1.18	1.48	0.35	1.03	1.76	1.25	1.69	Training
Chloridazon	1.76	1.14	0.18	1.32	1.76	1.63	1.52	Training
Chloroxylenol	0.68	0.31	0.72	0.37	0.96	0.98	1.18	Validation
Cimetidine	2.85	2.33	0.59	2.27	2.41	1.43	1.96	Validation
Clofibric Acid	0.64	1.01	0.50	0.66	1.11	0.93	1.54	Training
Codeine	2.85	2.80	0.26	1.53	2.16	1.91	2.21	Training
Cotinine	1.56	0.61	0.00	1.21	1.46	1.15	1.39	Validation
DEET	1.33	1.17	0.00	0.84	1.42	0.93	1.68	Training
Diazinon	3.35	2.82	0.00	2.56	2.57	1.22	2.31	Training
Diclofenac	2.64	2.58	0.59	1.34	2.10	2.06	2.03	Training
Dimethoate	1.01	1.38	0.35	2.44	2.41	1.31	1.58	Training
Estrone	2.45	2.60	0.55	0.82	1.55	1.54	2.16	Training
Famotidine	3.47	3.38	0.73	2.09	2.79	2.50	2.26	Validation
Hydrocodone	2.89	2.68	0.00	1.52	2.31	1.74	2.21	Validation
Ibuprofen	1.98	1.47	0.59	0.49	0.83	0.75	1.78	Training
Imidacloprid	1.75	1.51	0.17	1.53	1.98	1.56	1.68	Training
Ioxynil	1.67	1.18	0.50	0.30	1.48	2.07	1.45	Validation
Ketoprofen	2.20	2.27	0.59	0.86	1.77	1.53	1.98	Training
Malaoxon	2.20	2.44	0.00	2.90	2.51	0.61	2.21	Training

MCPA	0.67	0.71	0.50	0.61	1.16	0.96	1.39	Validation
Mecoprop	0.42	1.02	0.50	0.63	1.12	0.95	1.54	Training
Meprobamate	0.52	1.37	0.91	0.68	0.58	0.48	1.73	Training
Methomyl	0.63	0.24	0.35	1.18	1.13	0.94	1.21	Validation
Metolachlor	2.50	2.57	0.00	0.72	1.67	1.19	2.28	Training
Metribuzin	1.36	1.07	0.00	1.60	1.32	1.15	1.62	Validation
Morphine	2.43	2.60	0.55	1.54	2.06	1.99	2.06	Training
Nadolol	2.84	3.39	0.70	1.87	1.62	1.51	2.49	Validation
Naproxen	2.56	1.77	0.59	0.74	1.40	1.52	1.78	Training
Oxcarbazepine	1.83	2.11	0.35	1.00	2.03	2.01	1.87	Training
Paraxanthine	0.08	0.62	0.35	2.24	2.17	1.56	1.22	Training
Penciclovir	2.79	2.46	1.23	2.84	2.69	2.05	1.80	Training
Pentoxyfylline	1.75	2.24	0.00	1.65	1.47	1.73	2.08	Training
PFOA	-0.03	0.51	0.83	0.33	-0.10	-0.99	1.58	Validation
Phenytoin	1.67	2.30	0.60	2.02	2.19	2.23	1.87	Validation
Progesterone	2.96	3.26	0.00	0.89	1.43	1.19	2.62	Training
Propachlor	1.46	1.20	0.00	0.52	1.54	1.16	1.66	Training
Ranitidine hcl	2.20	3.05	0.20	1.93	1.92	1.54	2.4	Training
Siduron	2.62	2.02	0.44	1.20	1.36	1.34	1.95	Training
Simazine	1.38	1.10	0.65	2.16	1.55	1.23	1.48	Training
Sulfamethoxazole	1.78	1.98	0.61	1.17	2.73	1.82	1.72	Training
Sulfathiazole	1.40	2.00	0.61	1.33	2.71	2.17	1.69	Validation
TCEP	1.21	1.33	0.00	1.83	1.91	0.51	1.76	Validation
Testosterone	2.99	2.86	0.35	0.86	1.28	1.22	2.38	Training
Tributyl_phosphate	2.63	2.18	0.00	1.85	1.44	0.13	2.24	Training
Triclosan	2.72	1.92	0.41	0.26	1.84	1.81	1.81	Training
Trimethoprim	2.61	3.05	0.65	1.84	2.88	1.95	2.18	Validation
Warfarin	2.66	3.18	0.35	1.49	2.57	2.10	2.31	Training

a. The actual values $\log K_{\infty}$ calculated from the affinity experiments;
b. The predicted values $\log K_{\infty}$ calculated from reduced LSER model;
c. The solvatochromic descriptors (α^H, β^H, π^H, R, V) were calculated with PaDEL-Descriptor developed by the National Singapore University.

D. Data of kinetic and instantaneous uptake experiments

Table D1: Results of kinetics experiments and instantaneous uptake experiments.

No.[a]	**k_{obs}, [g mg^{-1} min^{-1}]**[b]		**R: 5 min, [%]**[c]		**R: 30 min, [%]**[c]		**Instant Uptake, [%]**	
	CCAC	P-CDP	CCAC	P-CDP	CCAC	P-CDP	CCAC	P-CDP
1	11.0	0.0 (72.9)	43.3±3.4	2.2±5.0	76.8±1.6	4.7±3.0	43.4±4.1	3.7±4.8
2	14.0	141.8	56.2±2.7	90.4±3.9	88.1±1.9	94.6±0.3	50.8±0.3	98.9±5.2
3	1.9	586.88	61.2±4.4	64.1±16.1	97±0.6	82.6±10.1	72.5±0.0	99.9±5.2
4	13.9	0.0 (-772.6)	32.4±7.6	6.8±2.8	56.1±6.9	0.6±1.8	57.8±9.0	0.0±3.9
5	13.0	61.9	59.7±4.5	51.7±4.1	90.9±0.8	59.3±2.1	53.5±5.7	66.0±4.5
6	0.0 (-1775.1)	151.0	0.0±9.0	74.2±3.9	0.2±6.1	79.2±4.3	23.5±1.9	91.8±10.0
7	26.4	37.3	32.9±11.0	1.1±13.1	47.5±4.8	6.3±3.6	53±13.1	0±7.0
8	0.0 (-4485.5)	73712.2	0±7.1	75.5±16.5	0±11.2	72.4±9.9	33.4±0.7	97.1±9.0
9	5.0	182.8	16.7±8.1	83.3±6.6	45.2±4.3	88.5±2.1	44.4±0.6	97.1±5.8
10	16.3	85.7	34.6±1.5	76.4±3.9	57.8±3.6	82.3±2.0	42.3±1.2	94.2±4.8
11	14.7	177.1	44.6±1.5	17.6±4.8	75.7±1.7	22.2±4.9	43.7±4.8	29.2±6.0
12	21.0	281.1	60.4±1.8	15.5±2.1	82.9±1.0	18.2±5.0	56.2±4.4	27.1±5.6
13	16.9	612.7	39.4±2.6	8.7±4.3	64.2±2.8	8.8±6.07	44.7±4.1	6.9±4.4
14	3.1	5184.7	20.7±2.6	59.6±13.1	67.0±6.4	71.6±4.1	46.6±0.1	99.7±5.8
15	13.0	207.9	44.7±19.0	0.7±6.7	77.5±3.4	5.5±6.5	61.1±12.1	0.0±6.4
16	13.0	335.1	56.2±5.4	15.1±2.9	86.3±1.4	18.0±3.6	56.3±1.8	26.6±4.7
17	16.8	1485.8	49.0±1.8	11.3±3.9	77.2±1.5	12.7±6.3	49.6±1.8	17.7±7
18	15.2	0.0 (-980.1)	40.3±1.9	4.8±1.6	67.3±2.2	3.2±5.6	45.3±1.8	4.9±5.5
19	14.3	364.9	56.6±5.7	23.9±2.6	86.3±1.6	25.4±2.9	54.7±6.2	29.6±5.9
20	10.6	52.8	47.4±4.9	10.1±15.5	77.9±1.0	19±16.4	45.4±7.2	7.5±3.6
21	18.7	100.9	58.8±6.9	86.5±5.3	85.5±1.3	92.4±0.5	56.5±0.5	99.8±3.1
22	16.8	0.0 (-112.9)	36.8±3.1	2.5±5.6	60.4±0.5	4.5±7.3	35.4±1.2	2.3±2.4
23	19.8	1501.2	22.2±6.9	90.6±12.7	59.8±4.2	94.3±1.3	41.2±0.3	100±5.7
24	17.8	239.3	32.1±9.5	26.8±5.1	50.3±1.7	25.2±4.0	40.6±5.6	42±6.3
25	16.8	577.9	39.0±1.1	12.1±2.8	66.7±3.1	13±2.9	42.6±3.2	20.5±4.6
26	26.3	194.7	72.5±1.4	90.3±5.3	96.8±0.0	94.6±0.9	60.3±0.4	98.4±6.3
27	6.4	46.4	48.0±3.7	32.4±4.4	88.1±1.5	40.4±2.8	43.1±3.5	77.8±3.9
28	11.1	0.0 (-248.1)	21.5±22.0	7.0±4.4	55.6±8.5	4.9±8.2	50.3±10.2	9.3±9.3
29	21.8	122.4	75.9±2.0	81.6±3.5	96.7±0.3	86.8±1.0	63.6±1.5	93.4±5.6
30	25.1	170.6	65.2±4.3	82.0±6.0	95.7±0.4	87.9±1.0	56.8±1.3	95.0±6.4
31	14.4	171.9	39.1±8.2	60.6±13.2	92.6±2.8	79.4±3.7	68.4±0.0	100±6.8

32	16.8	67.4	66.2±2.9	55.5±5.3	96.2±0.5	64.9±4.1	61.1±4.2	73.4±3.9
33	26.1	107.4	74.2±4.0	87.4±6.2	95.5±0.3	93.1±0.7	63.4±0.3	99.3±2.5
34	11.8	329.4	43.5±2.4	6.5±4.7	74.3±1.7	7.8±2.7	51.8±3.4	5.7±5.5
35	2563.0	137.0	12.3±37.0	46.8±10.7	71.2±7.7	66.3±6.4	79.2±0.0	100±5.53
36	8.1	143.0	54.6±4.3	76.1±7.7	93.9±1.3	79.2±5.4	47.7±0.6	97.8±4.2
37	16.7	1506.9	22.2±6.9	89.8±14.8	59.8±4.2	94.1±1.7	40.3±0.3	98.6±5.6
38	2.9	43.7	20.9±4.1	9.1±7.5	62.5±3.9	25.5±10.7	38.2±9.3	48.7±6.6
39	15.1	224.8	56.8±1.6	26.9±3.3	85.8±1.6	29.3±2.6	53.1±3.9	39.4±4.4
40	5.0	73.9	32.0±10.5	6.9±6.5	72.4±7.7	7.7±7.3	57.5±13.2	1.8±2.4
41	6.8	9915.0	47.2±4.7	7.3±4.8	85.9±0.2	8.2±3.4	50.8±3.9	57.5±2.6
42	15.3	84.6	55.9±3.4	61.0±4.1	86.1±1.5	67.9±2.1	54.3±4.5	75.1±4.3
43	8.6	268.7	49.8±5.1	23.8±2.9	87.2±1.3	25.3±4.5	43.8±5.1	68.7±4.4
44	24.4	143.3	77.3±3.7	89.0±4.1	97.5±0.1	93.4±0.7	64.3±0.6	97.2±5.0
45	12.7	359.4	46.8±1.9	24.4±3.0	78.0±2.2	25.6±3.9	49.3±4.7	44.0±4.8
46	11.9	0.0 (255.6)	43.8±2.6	0.0±4.6	74.8±0.9	1.2±5.6	42.2±2.9	7.6±3.6
47	11.2	0.0 (1997.2)	38.8±1.2	0.0±2.3	74.0±1.6	0.0±7.0	40.6±3.8	3.7±2.4
48	15.9	0.0 (-405.0)	34.9±4.7	5.1±6.1	57.5±2.2	2.2±4.3	48.1±8.3	3.1±7.7
49	17.6	0.0 (-98.6)	24.7±7.6	0.0±10.3	47.1±6.3	0.0±11.4	53.9±10.3	0.0±3.7
50	11.9	59.5	58.6±2.9	56.7±4.6	91.1±1.2	64.3±2.2	53.6±5.0	71.4±4.2
51	1.7	1633.2	40.0±3.9	85.8±20.1	83.3±3.1	91.1±2.8	60.6±0.1	99.7±6.0
52	18.8	435.3	36.8±0.9	12.7±3.2	58.9±2.5	13.6±4.5	41.9±3.8	17.8±5.5
53	15.5	212.6	52.7±2.5	32.4±2.8	79.3±1.8	35.9±3.4	51.0±5.7	47.7±4.9
54	3.1	162.1	15.2±13.0	80.5±5.2	41.8±3.0	86.3±2.9	45.3±1.0	96.1±3.0
55	2.2	197.6	31.1±1.8	85.9±7.8	69.5±5.0	91.4±2.0	56.0±0.3	98.5±4.9
56	10.5	57.3	52.5±4.0	41.0±6.1	89.2±1.0	51.7±7.0	43.3±2.1	88.9±4.9
57	14.5	60.3	59.9±4.5	12.1±11.1	90.3±5.0	20.8±2.6	52.1±1.8	14.6±4.9
58	116.1	927.3	91.5±2.3	94.7±15.4	99.4±0.0	92.8±6.8	76.4±0.2	99.6±5.3
59	15.3	0.0 (60.9)	47.5±8.0	0.1±5.2	71.8±4.7	2.4±7.1	58.2±6.7	5.6±6.0
60	16.3	102.7	57.8±6.9	87.4±4.9	88.2±2.9	92.8±0.6	59.1±0.2	98.6±4.2
61	13.7	1780.0	62.4±6.9	25.6±2.4	94.7±0.4	23.8±3.9	55.9±6.3	33.1±5.3
62	29.0	0.0 (6538.3)	20.5±5.9	0.0±5.3	32.3±4.4	0.3±7.8	28.2±5.4	8.4±7.7
63	9.9	0.0 (-10733.6)	39.0±5.5	0.0±6.3	71.5±1.1	0.0±4.0	35.4±3.1	8.0±4.0
64	11.0	244.0	44.4±12.0	19.2±6.2	78.9±2.5	22.1±5.8	47.9±4.7	31.7±5.9
65	43.7	222.3	84.7±1.7	94.1±3.8	99.3±0.1	97.0±0.1	74.2±0.2	99.3±4.7
66	14.4	179.5	40.4±2.5	91.5±4.0	73.0±1.8	95.1±1.1	42.7±0.5	97.9±3.8
67	17.0	2055.4	43.6±1.3	14.4±4.0	70.2±1.8	16.0±2.9	45.1±6.7	23.1±4.6
68	16.5	9346.4	41.5±4.5	71.2±3.6	84.4±4.2	72.0±0.3	42.2±0.2	99.3±15

69	14.3	73.7	63.2±3.4	62.6±3.2	92.5±0.9	70.2±1.9	55.9±3.8	78.5±4.7
70	18.3	1477.0	68.6±3.7	11.3±3.9	95.0±0.5	12.7±6.3	58.2±3.1	82.6±6.2
71	2.0	1538.2	53.6±3.6	62.6±12.3	93.7±1.2	72.5±2.5	69.0±0.0	99.9±5.4
72	10.3	114.0	38.6±18	13.9±10.9	74.5±2.7	14.1±10.0	53.9±12.2	10.8±4.1
73	10.0	341.5	35.9±14.0	25.7±3.6	71.1±4.1	26.9±3.8	43.4±5.0	41.7±4.5
74	10.4	1097.2	50.7±7.7	14.3±4.6	83.2±2.8	15.9±2.7	53.0±2.6	20.9±3.6
75	15.1	240.2	41.2±0.5	10.9±2.7	66.9±2.4	12.8±3.5	48.9±5.4	15.7±6.1
76	16.5	74.3	71.1±2.9	79.5±4.2	98.4±0.2	86.4±1.3	60.8±2.2	91.2±4.6
77	5.1	5239.8	11.5±1.8	66.6±12.1	46.5±6.4	81.0±6.7	38.1±0.2	99.4±5.3
78	12.1	55.6	60.2±3.1	61.4±5.7	92.6±1.2	70.5±2.1	55.0±3.2	82.5±5.6
79	264.0	753.4	92±2.3	92.3±7.1	99.5±0.0	95.3±0.8	79.6±0.1	99.7±2.5
80	14.3	898.8	55.5±2.5	95.1±10.5	90.9±1.5	97.9±0.3	65.6±0.0	100±5.3
81	3.8	87.2	28.5±2.1	12.5±3.1	73.7±0.8	18.0±5.1	27.5±2.6	73.7±3.4
82	5.5	5259.9	13.9±2.5	59.8±17.6	51.8±6.3	72.9±5.2	38.9±0.2	99.4±6.0
83	6.3	35.5	41.9±4.0	46.5±3.6	84.3±1.7	58.2±2.9	37.9±5.2	73.2±2.1

a. Number was used to represent the respective MP with reference to the identification tag provided in Appendix A;
b. k_{obs} (g mg^{-1} min^{-1}) was calculated with Ho and McKay pseudo second model;
c. R represents removal percentage relative to control experiments.

E. Results of LSER model

Table E1: Summary table of the full model with all 5 solvatochromic descriptors *(α^H, β^H, π^H, R, V)*

Descriptors	**Coefficients[a]**	**Std. Error[b]**	**t value[c]**	**Pr (> | t |)[d]**
Intercept	-2.9622	0.4800	-6.172	5.16e-07
MV (*V*)	2.1530	0.2167	9.937	1.37e-11
AC (α^H)	0.4085	0.2743	1.489	0.146
BH (β^H)	0.0128	0.1395	0.092	0.927
Pi (π^H)	0.1810	0.2354	0.769	0.447
ER (*R*)	0.2576	0.2144	1.202	0.238

a. Regression coefficients represent the mean change in the response variable ($\log K_\infty$) for one unit of change in the descriptor (α^H, β^H, π^H, *R* or *V*) while holding other descriptors as constants;
b. The standard error is an estimate of the standard deviation of respective regression coefficient;
c. The t value is the coefficient divided by its standard error;
d. The p-value is determined by comparing the t value to the respective t distribution and small p-value indicates high significance of the regression coefficient.

Table E2: Summary table of the reduced model with 4 solvatochromic descriptors *(α^H, π^H, R, V)*

Descriptors	**Coefficients**	**Std. Error**	**t value**	**Pr (> | t |)**
Intercept	-2.9615	0.4731	-6.260	3.51e-07
MV (*V*)	2.1529	0.2136	10.081	6.86e-12
AC (α^H)	0.4128	0.2664	1.550	0.130
Pi (π^H)	0.1956	0.1715	1.140	0.262
ER (*R*)	0.2504	0.1968	1.273	0.212

Table E3: Analysis of variance table of 5 solvatochromic descriptors *(α^H, β^H, π^H, R, V)*

Descriptors	**Degree of freedom[a]**	**Sum of Square[b]**	**Mean of Square[c]**	**F value[d]**	**Pr (> F)[e]**
MV (*V*)	1	24.0007	24.0007	115.5927	1.77e-12
AC (α^H)	1	0.9041	0.9041	4.3543	0.0445
BH (β^H)	1	02108	02108	1.0151	0.3208
Pi (π^H)	1	0.7573	0.7573	3.6474	0.0646
ER (*R*)	1	0.2999	0.2999	1.4443	0.2378
Residuals	34	7.0595	0.2076		

a. The degree of freedom of the respective descriptor;
b. The sum of square indicates the variation attributed to the respective descriptor;
c. The mean of square is the sum of square divided by the degree of freedom of the respective descriptor;
d. The F value is the mean of square of the descriptor divided by that of the residuals;
e. The p-value is determined by comparing the F value to the respective F distribution and small p-value indicates high influence of the descriptor.

Table E4: Analysis of variance table of the full model and the reduced model

Model	Residual Degree of freedom	Residual Sum of Square	Degree of freedom[a]	Sum of Square[b]	F value[c]	Pr (> F)[d]
Reduced	35	7.0612	----	------	----	----
Full	34	7.0595	1	0.0018	0.0085	0.9272

a. The difference between the degree of freedom of the full model and the reduced model;
b. The difference between the residual sum of square of the full model and the reduced model;
c. The F value is the value calculated in b. divided by the mean residual sum of square of the reduced model;
d. The p-value is determined by comparing the F value to the respective F distribution and small p-value indicates high influence of the descriptor.